Vol. 43 — N° 3 09 19 p. 355 – 384

GEOSTANDARDS and GEOANALYTICAL RESEARCH

Natural Titanite Reference Materials for *In Situ* U-Pb and Sm-Nd Isotopic Measurements by LA-(MC)-ICP-MS

Qian **Ma** (1, 2), Noreen J. **Evans** (3), Xiao-Xiao **Ling** (2, 4), Jin-Hui **Yang** (2, 4), Fu-Yuan **Wu** (2, 4), Zhi-Dan **Zhao** (1)* and Yue-Heng **Yang** (2, 4)*

(1) State Key Laboratory of Geological Processes and Mineral Resources, School of Earth Science and Resources, China University of Geosciences, Beijing 100083, China
(2) State Key Laboratory of Lithospheric Evolution, Institute of Geology and Geophysics, Chinese Academy of Sciences, Beijing 100029, China
(3) School of Earth and Planetary Science, John de Laeter Centre, Curtin University, Perth, WA, Australia
(4) Institutions of Earth Science, Chinese Academy of Sciences, Beijing 100029, China
* Corresponding authors. e-mails: zdzhao@cugb.edu.cn and yangyueheng@mail.iggcas.ac.cn

Titanite is a common accessory mineral that preferentially incorporates considerable amounts of U and light rare earth elements in its structure, making it a versatile mineral for *in situ* U-Pb dating and Sm-Nd isotopic measurement. Here, we present *in situ* U-Pb ages and Sm-Nd isotope measurement results for four well-known titanite reference materials (Khan, BLR-1, OLT1 and MKED1) and eight titanite crystals that could be considered potential reference material candidates (Ontario, YQ-82, T3, T4, TLS-36, NW-IOA, Pakistan and C253), with ages ranging from ~ 20 Ma to ~ 1840 Ma. Results indicate that BLR-1, OLT1, Ontario, MKED1 and T3 titanite have relatively homogeneous Sm-Nd isotopes and low common Pb and thus can serve as primary reference materials for U-Pb and Sm-Nd microanalysis. YQ-82 and T4 titanite can be used as secondary reference materials for *in situ* U-Pb analysis because of their low common Pb. However, internal structures and mineral inclusions in YQ-82 will require careful selection of suitable target domains. Pakistan titanite is almost concordant with an age of 21 Ma and can be used as a reference material when dating Cenozoic titanite samples.

Keywords: titanite, reference material, LA-(MC)-ICP-MS, Sm-Nd isotopes, U-Pb geochronology, *in situ* analysis.

Received 18 Dec 18 – Accepted 12 Mar 19

Titanite (sphene), $Ca(Ti,Al,Fe^{3+})SiO_4(O,OH,F)$, is a common accessory mineral in a wide variety of felsic and intermediate igneous, low- to high-grade metamorphic, sedimentary and hydrothermal ore deposit-related rocks (Frost *et al.* 2000, Kohn 2017). Titanite usually incorporates variable amounts of U (10–1000 μg g^{-1}) and Th (10–1000 μg g^{-1}), but exhibits a lower incidence of radiation damage relative to zircon which typically has 5–10 times higher abundances of parent isotopes (Tilton and Grunenfelder 1968). Titanite remains closed to complete Pb loss at temperatures as high as 660–750 °C (Cherniak 1993, Scott and St-Onge 1995, Spencer *et al.* 2013), making it an attractive mineral for U-Pb dating. Although zircon is the most accessible and common choice for dating crystallisation due to its physical and chemical resistance during post-crystallisation thermal and chemical geological processes, titanites are relatively reactive during metamorphism and hydrothermal events, and therefore, a titanite date reflects the latest process that disturbed the U-Pb system. Titanite U-Pb geochronology has been used predominantly to study igneous, metamorphic and hydrothermal processes (Tucker *et al.* 1987, Corfu 1996, Li *et al.* 2010, Rasmussen *et al.* 2013, Xu et al. 2015a). U-Pb titanite ages are especially useful when combined with zircon ages (or other geochronometers with different closure temperatures for Pb) to define temperature–time histories (Schaltegger *et al.* 2009, Chew *et al.* 2014). Furthermore, titanite always contains an enrichment of the light rare earth elements (LREE) Sm and Nd in its lattice (Tiepolo *et al.* 2002, Prowatke and Klemme 2005, Xie *et al.* 2010). Due to the high closure temperature of Nd (850–950 °C) in titanite, the original Nd isotopic composition can be preserved, even during high-temperature thermal events (Cherniak 1995). Linking *in situ* titanite U-Pb dating with Sm-Nd isotopic data can provide a valuable insight into the origin and evolution of

doi: 10.1111/ggr.12264

magma, fluids and metamorphic processes (Amelin 2009, Gregory *et al.* 2009, Cao *et al.* 2015).

The U-Pb age and Sm-Nd composition can be obtained using conventional isotope dilution thermal ionisation mass spectrometry (ID-TIMS), which is regarded as the benchmark technique for U-Pb and Sm-Nd isotopic analysis. However, bulk analysis of single crystals can obscure micro-geological information since chemical and isotopic zonation is common in natural titanite (e.g., < 100 μm inherited cores and metamorphic zonation; Jiang *et al.* 2016, Marsh and Smye 2017). *In situ* U-Pb analytical techniques such as secondary ion mass spectrometry (SIMS; Heaman 2009, Bonamici *et al.* 2015) and laser ablation-inductively coupled plasma-mass spectrometry (LA-ICP-MS; Willigers *et al.* 2002, Simonetti *et al.* 2006, Banerjee *et al.* 2007, Burn *et al.* 2017) can be applied to titanite to capture heterogeneities within single grains. LA-ICP-MS U-Th-Pb dating is widely adopted because of its good spatial resolution (20–50 μm), adequate precision (typically < 3% on individual $^{206}Pb/^{238}U$ and $^{208}Pb/^{232}Th$ measurement), rapid analysis (in the order of several minutes) and low cost compared with other microanalytical techniques (e.g., SIMS; Storey *et al.* 2006, Fu *et al.* 2016). Meanwhile, *in situ* Sm-Nd isotopic analysis by multi-collector (MC) ICP-MS has also been recently proved feasible for titanite as well as other LREE-enriched accessory minerals (Foster and Vance 2006, McFarlane and McCulloch 2007, Yang *et al.* 2008, Gregory *et al.* 2009, Fisher *et al.* 2011). Both SIMS and LA-(MC)-ICP-MS are relative methods, and a matrix-matched mineral reference material is required for calibration during measurement sessions. Employing matrix-matched calibration can significantly minimise the laser-induced matrix effects, resulting in more precise and accurate U-Pb ages and Sm-Nd measurement results (Xie *et al.* 2018 and references therein).

Although there are numerous well-characterised zircon, monazite, apatite and rutile reference materials for U-Pb, Hf, Nd and/or Sr isotopic analysis (Wu *et al.* 2006, Fisher *et al.* 2011, Iizuka *et al.* 2011, Liu *et al.* 2012, Yang *et al.* 2014, Li *et al.* 2015), there are relatively few established titanite reference materials (e.g., Khan, BLR-1, OLT1 for U-Pb dating and MKED1 for U-Pb and Sm-Nd isotope microanalysis), and with the advent of high-throughput *in situ* analytical methods, demand for titanite geochronology reference materials is outstripping supply. Moreover, the growing application of *in situ* titanite Sm-Nd isotope measurement by LA-(MC)-ICP-MS has created a need for a range of homogeneous Sm-Nd reference materials. Few publications report Sm-Nd isotopic data for the available titanite reference materials. Recently, Spandler *et al.* (2016) reported the first Sm-Nd isotope data for titanite MKED1 (ID-TIMS and LA-MC-ICP-MS. More recently, Xu *et al.* (2015b, 2018) also reported Sm-Nd isotope data for Khan, BLR-1 and OLT1 using LA-MC-ICP-MS with no results by the solution method. Some workers have demonstrated that using a matrix-matched reference material is essential for precise and accurate $^{147}Sm/^{144}Nd$ measurement (Iizuka *et al.* 2011, Liu *et al.* 2012, Yang *et al.* 2014); however, the approach to correction for isotopic fractionation varies. Fisher *et al.* (2011) used LREE glass to calibrate $^{147}Sm/^{144}Nd$, similar to the method conducted by Foster and Vance (2006) who used the $^{147}Sm/^{144}Nd$ ratio of NIST SRM 610 determined by isotope dilution as the 'external' reference value.

Bearing this consideration in mind, we have undertaken a comprehensive examination of the U-Pb age and Sm-Nd isotopic composition of twelve natural titanite crystals, including four well-characterised reference materials (Khan, BLR-1, OLT1 and MKED1) and eight candidate reference materials (Ontario, YQ-82, T3, T4, TLS-36, NW-IOA, Pakistan and C253). The aim is to find suitable titanite reference materials for *in situ* Sm-Nd measurement and U-Pb age measurement so that a suite of well-calibrated titanite materials can be made available to the geochemical research community.

Analytical methods

Electron probe microanalysis

Backscattered electron (BSE) imaging of titanite was undertaken using a Nova NanoSEM 450 field-emission scanning electron microscope (FSEM) to characterise internal structures and mineral inclusions. Quantitative major element determination in titanite minerals was performed on a JEOL JXA-8100 and CAMECA SXFive electron microprobe housed at the Electron Microprobe and Scanning Electron Microscope Laboratory, Institute of Geology and Geophysics (IGG), Chinese Academy of Sciences (CAS), Beijing. The operating conditions included beam currents of 2×10^{-8} and 3×10^{-8} A for the JEOL JXA-8100 and CAMECA SXFive instruments, respectively, where both instruments used an accelerating voltage of 15 kV and a beam size of 5 μm. The peak counting time was 20 s for all elements and the background counting time was 10 s on the high- and low-energy background positions. Natural minerals, synthetic oxides and glasses were used as reference materials. Results of major element compositions are presented in Table 1.

In situ trace element measurement and U-Pb age determination

An Agilent 7500a Q-ICP-MS instrument coupled to a 193 nm ArF excimer laser ablation system housed at

Table 1.
Major element composition (% *m/m*) of titanites in this study

Titanite	Khan (*n* = 10)		BLR-1* (*n* = 15)		OLT1* (*n* = 15)		Ontario* (*n* = 16)		MKED1 (*n* = 10)		YQ-82 (*n* = 10)		T3* (*n* = 15)		T4* (*n* = 15)		TLS-36 (*n* = 10)		NW-IOA (*n* = 10)		Pakistan* (*n* = 15)		C253 (*n* = 10)	
	Mean	2*s*	Mean	2*s*	Mean	2*s*	Mean	2*s*	Mean	2*s*	Mean	2*s*	Mean	2*s*	Mean	2*s*	Mean	2*s*	Mean	2*s*	Mean	2*s*	Mean	2*s*
SiO_2	30.06	0.55	29.78	0.28	29.99	0.24	29.77	0.20	30.63	0.46	30.74	0.42	28.82	0.37	30.02	0.35	30.14	0.44	30.45	0.49	30.09	0.47	30.75	0.30
TiO_2	33.23	0.80	33.01	0.24	29.68	0.24	32.84	0.35	36.09	0.63	37.11	0.80	34.56	0.79	39.17	0.92	35.60	0.53	35.10	0.61	38.37	0.64	37.43	0.79
Al_2O_3	2.46	0.18	3.13	0.08	4.83	0.08	2.72	0.09	1.35	0.12	1.18	0.39	1.13	0.10	0.68	0.24	1.20	0.16	1.36	0.37	1.72	0.08	0.99	0.03
Fe_2O_3	1.44	0.13	2.40	0.12	2.64	0.07	2.91	0.16	1.53	0.12	0.84	0.22	3.28	0.44	0.85	0.42	1.57	0.26	1.92	0.37	0.23	0.06	0.64	0.06
MnO	0.12	0.08	0.11	0.03	0.03	0.03	0.11	0.04	0.03	0.05	0.03	0.04	0.06	0.04	0.02	0.02	0.15	0.06	0.04	0.05	0.01	0.01	0.03	0.03
MgO	0.04	0.05	0.07	0.01	0.10	0.02	0.07	0.01	0.01	0.01	0.01	0.01	0.01	0.02	0.01	0.01	0.02	0.02	0.02	0.02	0.02	0.01	0.02	0.03
CaO	26.37	0.49	27.36	0.24	27.80	0.28	27.38	0.22	27.42	0.36	27.62	0.63	25.32	0.65	28.48	0.35	26.69	0.65	27.43	0.49	28.80	0.34	27.59	0.43
Na_2O			0.22	0.03	0.05	0.02	0.20	0.03					0.08	0.02	0.03	0.03					0.07	0.03		
P_2O_5	0.08	0.09	0.06	0.02	0.05	0.02	0.05	0.02	0.05	0.07	0.07	0.07	0.07	0.03	0.07	0.05	0.11	0.04	0.04	0.07	0.06	0.04	0.08	0.06
Y_2O_3	0.41	0.26	0.42	0.06	0.13	0.03	0.38	0.06	0.13	0.17	0.33	0.42	2.28	0.22	0.09	0.11	0.16	0.17	0.13	0.14	0.06	0.04	0.10	0.16
PbO	0.06	0.08							0.05	0.07	0.06	0.09					0.13	0.17	0.11	0.13			0.07	0.10
ThO_2	0.11	0.11							0.10	0.13	0.05	0.08					0.08	0.15	0.06	0.09			0.04	0.08
UO_2	0.11	0.14							0.04	0.06	0.05	0.07					0.07	0.10	0.09	0.16			0.05	0.06
La_2O_3	0.20	0.13	0.05	0.03	0.09	0.02	0.05	0.04	0.10	0.14	0.02	0.02	0.25	0.09	0.16	0.14	0.26	0.19	0.10	0.09	0.02	0.02	b.d.	–
Ce_2O_3	b.d.	–	0.38	0.03	0.53	0.03	0.37	0.04	b.d.	–	b.d.	–	1.08	0.27	0.51	0.17	0.32	0.40	b.d.	–	0.26	0.04	b.d.	–
Ta_2O_5	0.21	0.29	0.06	0.10	0.07	0.09	0.08	0.12	0.16	0.23	0.16	0.22	0.16	0.22	0.05	0.06	0.13	0.14	0.25	0.26	0.09	0.10	0.22	0.31
V_2O_3	b.d.	–							b.d.	–	0.02	0.02					b.d.	–	0.12	0.14			0.01	0.01
ZrO_2	0.07	0.08	0.19	0.06	0.20	0.06	0.17	0.10	0.05	0.06	0.01	0.00	0.04	0.05	0.05	0.08	0.08	0.13	0.12	0.19	0.05	0.07	0.08	0.07
Pr_2O_3	0.07	0.14							0.08	0.13	0.15	0.15					0.14	0.17	0.09	0.18			0.09	0.11
Nb_2O_5	0.75	0.31	0.59	0.12	0.94	0.12	0.63	0.12	0.16	0.14	0.08	0.09	0.49	0.90	0.07	0.12	0.21	0.21	0.08	0.16	0.30	0.15	0.09	0.10
Nd_2O_3	0.33	0.11	0.20	0.07	0.28	0.10	0.17	0.06	0.15	0.16	0.13	0.19	0.63	0.21	0.10	0.10	0.39	0.24	0.15	0.19	0.06	0.08	0.07	0.09
Gd_2O_3			0.10	0.06	0.07	0.07	0.07	0.09					0.39	0.13	0.07	0.11					0.05	0.05		
Eu_2O_3	0.06	0.07							0.05	0.07	0.04	0.06					0.08	0.14	0.03	0.05			0.04	0.06
Sm_2O_3	0.06	0.09	0.06	0.08	0.06	0.09	0.08	0.12	0.08	0.12	0.09	0.11	0.16	0.14	0.06	0.09	0.10	0.12	0.07	0.11	0.07	0.10	0.06	0.09
F	0.48	0.10	1.21	0.04	1.65	0.09	1.14	0.05	0.32	0.07	0.10	0.08	b.d.	–	0.04	0.05	0.10	0.10	0.30	0.18	0.46	0.05	0.27	0.14
Total	96.27	1.38	99.15	0.58	99.13	0.71	98.84	0.59	97.98	1.10	98.39	1.08	98.40	1.02	100.32	1.39	97.36	0.99	97.41	1.22	100.67	1.24	98.11	1.12
O=F	0.20	0.04	0.51	0.02	0.69	0.04	0.48	0.02	0.13	0.03	0.04	0.03	b.d.	–	0.02	0.02	0.04	0.04	0.13	0.07	0.19	0.02	0.11	0.06
Total	96.07	1.39	98.64	0.58	98.44	0.69	98.36	0.60	97.85	1.11	98.35	1.05	98.40	1.02	100.21	1.40	97.21	1.02	97.29	1.27	100.48	1.22	98.00	1.11
Fe/Al	0.37	0.04	0.49	0.03	0.35	0.01	0.68	0.04	0.72	0.09	0.46	0.07	1.85	0.38	0.81	0.33	0.84	0.13	0.91	0.15	0.09	0.02	0.41	0.04

n = number of data; b.d. = below detection limit; all Fe are calculated as Fe^{3+}; O=F is calculated as F × 0.42. Data marked with an asterisk (*) are obtained by CAMECA SXFive, and others are measured by JEOL JXA-8100.

IGG-CAS was used to determine trace element compositions and U-Pb ages. GeoLas Pro and Analyte G2 excimer laser ablation systems were used in this study, descriptions of which can be found elsewhere (Sun *et al.* 2012, Huang *et al.* 2015).

Prior to analysis, the pulse/analogue (P/A) factor of the detector was calibrated using a standard tuning solution. During laser ablation, the instrument was optimised using the NIST SRM 610 glass reference material. Helium was used as the carrier gas and mixed with argon before entering the ICP torch. The parameters of the two gases were optimised to obtain stable maximum signal intensity for $^{238}U^{+}$, while suppressing oxide formation and limiting fractionation between U and Th, which were monitored using the ThO^{+}/Th^{+} (< 0.5%) and Th/U (to *ca.* 1) ratios. Detailed parameter settings are presented in Table 2. A fluence of ~ 5 J cm^{-2}, a spot size of 40 μm and a repetition rate of 8 Hz were employed for measurement. All LA-ICP-MS measurements were carried out using time-resolved analysis in fast, peak jumping mode. The dwell time for each isotope was set at 6 ms for P, Rb, Sr, Ba, Nb, Ta, Zr, Hf and REEs; 10 ms for ^{232}Th and ^{238}U; 15 ms for ^{204}Pb, ^{206}Pb and ^{208}Pb; and 30 ms for ^{207}Pb. Each spot analysis consisted of an approximate 30 s background and a 60 s sample data acquisition. A matrix-matched titanite reference material (MKED1) was used to correct $^{207}Pb/^{206}Pb$, $^{206}Pb/^{238}U$, $^{207}Pb/^{235}U$ ($^{235}U = {}^{238}U/137.88$) and $^{208}Pb/^{232}Th$ ratios. Trace element mass fractions were calibrated using ^{43}Ca as the internal standard element (CaO mass fractions were measured previously by EPMA) using NIST SRM 610 as the calibrating reference material. Isotopic and elemental fractionation plus instrumental mass bias were calibrated using Glitter 4.0 software (Griffin *et al.* 2008). For multiple groups of reference materials, we selected the option for the interpolation of a linear fit to ratios to perform drift corrections. Signal sections of each analysis were selected independently to obtain a very similar interval for reference materials and unknowns. The relative standard deviation of reference values for MKED1 titanite was set at 2%. The U-Pb ages and weighted mean ages were calculated using the ISOPLOT 3.0 software package (Ludwig 2003).

In situ Sm-Nd isotope determination

All *in situ* isotopic measurements in this study were carried out at IGG-CAS, using a Thermo Scientific Neptune MC-ICP-MS coupled to a 193 nm excimer laser system. Detailed instrument and measurement conditions are presented in Table 2. Prior to analysis, the instrument was tuned and optimised for maximum sensitivity using the JNdi-1 standard solution. The laser fluence was set to ~ 6 J cm^{-2} with laser repetition rate and beam diameter set to 8 Hz and 60–120 μm, respectively, depending on the Nd mass fraction of the samples. Each spot analysis consisted of *ca.* 30 s of baseline acquisition and 60 s of data acquisition (Yang *et al.* 2008). Every ten sample analyses were followed by two MKED1 (or BLR-1/OLT1/Ontario) analyses for calibration.

To obtain accurate $^{147}Sm/^{144}Nd$ and $^{143}Nd/^{144}Nd$ isotopic ratios using LA-MC-ICP-MS, the contribution of the isobaric interference of ^{144}Sm on the ^{144}Nd signal must be carefully corrected (Foster and Vance 2006, McFarlane and McCulloch 2007, Fisher *et al.* 2011, Yang *et al.* 2008, 2009). In natural titanite, Sm/Nd generally ranges from 0.15 to 0.5, so ^{144}Sm can contribute ~ 2–6% to the measured ^{144}Nd signal. The Sm and Nd isotopic abundances of $^{147}Sm/^{149}Sm = 1.08680$, $^{144}Sm/^{149}Sm = 0.22332$ and $^{146}Nd/^{144}Nd = 0.7219$ (O'Nions *et al.* 1977, Dubois *et al.* 1992, Isnard *et al.* 2005) were adopted in this study. The measured $^{147}Sm/^{149}Sm$ was used to calculate a Sm fractionation factor using the exponential law. The measured ^{147}Sm intensity was used to estimate the Sm interference on mass 144 by employing the natural $^{147}Sm/^{144}Sm$ ratio of 4.866559 (Isnard *et al.* 2005). Then, the interference-corrected $^{146}Nd/^{144}Nd$ ratio was used to calculate the Nd fractionation factor. Finally, the $^{143}Nd/^{144}Nd$ and $^{145}Nd/^{144}Nd$ ratios were normalised using the exponential law. True $^{147}Sm/^{144}Nd$ ratio can also be calculated using the exponential law after correcting for the isobaric interference of ^{144}Sm on ^{144}Nd. The $^{147}Sm/^{144}Nd$ ratio was then calibrated against the $^{147}Sm/^{144}Nd$ ratio in a titanite reference material, analysed during the same session (Yang *et al.* 2013, 2014, Lin *et al.* 2016). The raw data were exported offline and the whole data reduction was performed using a Microsoft Excel macro written in VBA (Visual Basic for Applications).

Solution Sm-Nd isotope measurement

All titanite chemical preparation was undertaken on class 100 workbenches inside a class 1000 clean laboratory. Individual titanite crystal chips were washed in an ultrasonic bath in 2% HNO_3 for 15 min and then washed with Milli-Q water (18.2 MΩ cm at 25 °C; Millipore, Bedford, MA, USA) for several times. Each crystal was then dried. About 20–30 mg of titanite crystals was weighed into a 7 ml round-bottomed Savillex™ Teflon/PFA screw-top capsule. Each aliquot was spiked with a weighed ^{149}Sm-^{150}Nd-enriched tracer and then digested by concentrated $HClO_4$ and HF of 0.1 ml and 1 ml, respectively. The bulk rare earth elements were separated from other matrix elements using a standard cation exchange resin

Table 2.
Typical instrument parameters for U-Pb dating of titanite by LA-ICP-MS and Sm-Nd isotopic measurement by LA-MC-ICP-MS

Laser ablation systems	**Coherent GeoLas Plus**	**Analyte G2**
Laser system	COMPex 102, ArF excimer UV 193 nm	ATLex 300si, ArF excimer UV 193 nm
Ablation cell and volume	Standard circle low-volume cell, volume *ca.* 4 cm^3	Commercial HelEx dual-volume sample cell
Fluence	~ 5 J cm^{-2} for trace element and U-Pb dating, ~ 6 J cm^{-2} for Sm-Nd isotope	
Repetition rate	8 Hz	
Spot diameter nominal	40 μm for trace elements and U-Pb dating, 60–120 μm for Sm-Nd isotopes	
Ablation duration	60 s for trace elements and U-Pb dating, 80 s for Sm-Nd isotopes	
Sampling mode	Static spot ablation	
Sample preparation	Conventional mineral separation, 1 inch resin mount	

Mass spectrometers	**Thermo Fisher Neptune MC-ICP-MS**	**Agilent 7500a Q-ICP-MS**	
RF forward power (W)	~ 1300	RF forward power (W)	~ 1350
Cool gas (l min^{-1})	16	Carrier gas (l min^{-1})	~ 1.1
Auxiliary gas (l min^{-1})	0.8	Sample depth (mm)	~ 4.5
Carrier gas flow (l min^{-1})	~ 1.2	Interface cone	Ni
Sampling cone	Ni, aperture 1.0 mm	Dwell times	15 ms for ^{204}Pb, ^{206}Pb and ^{208}Pb, 30 ms for ^{207}Pb, 10 ms for ^{232}Th and ^{238}U, 6 ms for other elements
Skimmer cone	Ni, aperture 0.8 mm		
Sampling mode	9 blocks of 8 cycles for Nd (solution)		
	1 block of 40 cycles for Sm (solution)	Analysis duration	90 s (including 30 s background and 60 s ablation)
	1 block of 200 cycles (laser)		
Integration time	4 s for Nd (solution)		
	2 s for Sm (solution)		
	0.262 s (laser)		
Background/baseline	30 s on peak zero (OPZ)		

MC-ICP-MS cup configuration

Faraday cups	L4	L3	L2	L1	Centre	H1	H2	H3	H4
Nominal mass	142	143	144	145	146	147	148	149	150
Nd^+	$^{142}Nd^+$	$^{143}Nd^+$	$^{144}Nd^+$	$^{145}Nd^+$	$^{146}Nd^+$		$^{148}Nd^+$		$^{150}Nd^+$
$[Ce^+,Sm^+]$	$^{142}Ce^+$		$^{147}Sm^+$			$^{147}Sm^+$	$^{148}Sm^+$	$^{149}Sm^+$	$^{150}Sm^+$

Data processing

Gas blank	30 s on-peak zero subtracted
Calibration strategy	NIST SRM 610 used as reference material and ^{43}Ca used as internal standard for calibrating trace elements; MKED1 titanite used as primary reference material and BLR-1 titanite used as secondary RM for U-Pb dating; MKED1, BLR-1, OLT1 and Ontario used as Sm-Nd isotope reference materials
Reference material information (U-Pb dating)	MKED1 (Spandler *et al.* 2016), BLR-1 (Aleinikoff *et al.* 2007), OLT1 (Kennedy *et al.* 2010) and Ontario titanite (Spencer *et al.* 2013)

Table 2 (continued).
Typical instrument parameters for U-Pb dating of titanite by LA-ICP-MS and Sm-Nd isotopic measurement by LA-MC-ICP-MS

Data processing	
Reference material information (Nd isotope)	MKED1: $^{147}Sm/^{144}Nd$ = 0.1270, $^{143}Nd/^{144}Nd$ = 0.511630(03) (Spandler *et al.* 2016) BLR-1: $^{147}Sm/^{144}Nd$ = 0.1921, $^{143}Nd/^{144}Nd$ = 0.512815(04) (this study) Ontario: $^{147}Sm/^{144}Nd$ = 0.1928(11), $^{143}Nd/^{144}Nd$ = 0.512833(08) (this study)
Data processing package used	For trace elements and U-Pb data, Glitter software was used for isotopic and elemental fractionation, instrumental mass bias calibration, uncertainty propagation and age calculation. For Sm-Nd isotope, an in-house Microsoft Excel macro written in VBA (Visual Basic for Applications) was used for Nd isotope mass fraction correction, interference correction and uncertainty propagation
Common Pb correction	^{207}Pb correction is applied to the $^{206}Pb/^{238}U$ age data by ISOPLOT software
Uncertainty level	Ages are quoted at 2*s* absolute unless otherwise stated

(AG50W-X12, 2 ml, 200–400 mesh). Samarium (Sm) and Nd purification was achieved using a commercial Ln Spec resin column. The detailed sample digestion and separation protocol employed is described elsewhere (Yang *et al.* 2010, 2011).

Sm and Nd mass fractions and $^{143}Nd/^{144}Nd$ isotopic ratios were measured on a Thermo Fisher Scientific Neptune MC-ICP-MS at IGG-CAS. The operational settings and cup configurations are summarised in Table 2. The JNdi-1 Nd standard solution was used to evaluate the intermediate measurement precision and bias of the Sm-Nd isotopic measurement results. For Sm isotopic determination, the Alfa-Sm standard solution was used as a calibrator for mass bias correction of $^{147}Sm/^{149}Sm$ ratios. Detailed mass spectrometry and offline data reduction followed that given by Yang *et al.* (2011). Procedural blanks were < 50 pg for Sm and Nd. Therefore, the blank contribution was considered negligible and required no correction on the measured isotopic ratios.

The Sm and Nd mass fractions and Nd isotopic data of the replicate titanite crystals are presented in Table 4. In order to monitor analytical procedures, replicate analyses of certified reference materials BCR-2 and AGV-2 from the United States Geological Survey were conducted using the identical analytical procedure described above. During the period of data acquisition, BCR-2 and AGV-2 gave 0.512640 ± 0.000009 (2*s*, *n* = 3) and 0.512785 ± 0.000011 (2*s*, *n* = 2) for $^{143}Nd/^{144}Nd$ and 0.1376 ± 0.0017 (2*s*, *n* = 3) and 0.1089 ± 0.0001 (2*s*, *n* = 2) for $^{147}Sm/^{144}Nd$, respectively, identical within error to the recommended values (Weis *et al.* 2006, Chu *et al.* 2009, Yang *et al.* 2010, 2011).

Results

In this study, twelve titanites from different areas were investigated, with ages ranging from *ca.* 1840 to 20 Ma. Typical backscattered electron (BSE) images are presented in Figure 1. Major and trace element compositions of titanites are given in Tables 1 and 3, respectively, and chondrite-normalised REE patterns are shown in Figure 2. Sm and Nd mass fractions and $^{143}Nd/^{144}Nd$ isotopic ratios of titanite crystals acquired via solution methods are listed in Table 4. The *in situ* U-Pb and Sm-Nd data for the measured titanites are summarised in Tables 5 and 6, respectively. More detailed information of major and trace elements and U-Pb and Sm-Nd isotope data can be found in the online supporting information (Tables S1–S4).

For most titanites, Th-Pb ages are problematic for accurate dating because of the generally lower Th/U ratios

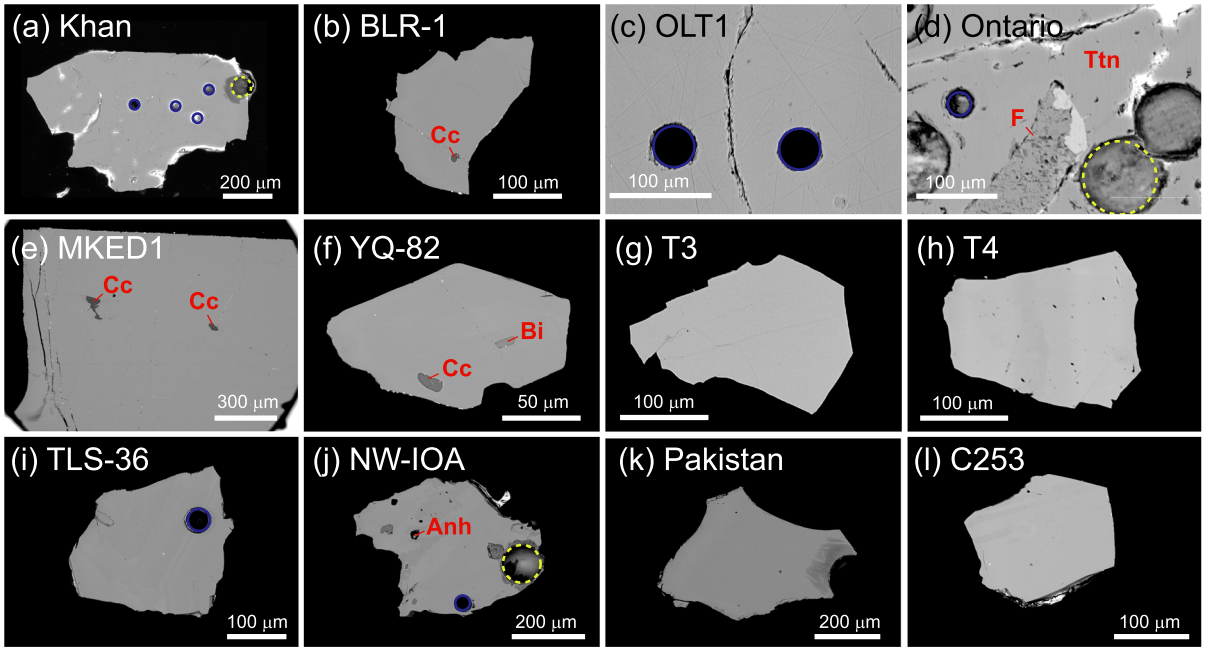

Figure 1. Representative BSE images for typical titanite crystals investigated in this study. Most Khan titanite crystals are relatively uniform, but some display numerous mineral inclusions. BLR-1 and MKED1 titanites are typically homogeneous in BSE images; however, calcite inclusions are visible in some grains; Ontario titanites are homogeneous in BSE images but contain mm-scale fluorite inclusions; most YQ-82 crystals contain abundant mineral inclusions; T3, T4, Pakistan and C253 titanites have homogeneous compositions; TLS-36 and NW-IOA titanites display some internal structures. Blue solid and yellow dashed circles indicate the locations of U-Pb and Sm-Nd laser spots, respectively. Anh = anhydrite; Bi = biotite; Cc = calcite; F = fluorite; and Ttn = titanite. [Colour figure can be viewed at wileyonlinelibrary.com]

(Th/U < 1) and higher f_{208} (common ^{208}Pb in proportion to total ^{208}Pb) compared with f_{206} (common ^{206}Pb in proportion to total ^{206}Pb), as shown in Figure 3a, b. Here, for titanites with common Pb, age calculations used a weighted mean of the ^{207}Pb-corrected ages and the Tera–Wasserburg (TW) concordia intercept age anchored through common Pb, based on the model of Stacey and Kramers (1975). For titanites with little common Pb, ^{207}Pb/^{235}U–^{206}Pb/^{238}U concordia diagrams are presented in this paper (Figure 4). The stable ^{145}Nd/^{144}Nd after isobaric interference correction can be used to evaluate both accuracy and reproducibility. Here, values of ^{145}Nd/^{144}Nd obtained via the laser ablation method were slightly higher than (mean values from 0.348424 to 0.348441; Table 6), but within measurement uncertainty of the reference value of 0.348415 acquired by TIMS (Wasserburg *et al.* 1981).

Khan

The Khan titanite was collected from a pegmatite sample exposed in the Khan copper mine, Namibia, south-west Africa. Previous work indicates that this titanite has some geochemical variability and displays considerable variation in ^{207}Pb/^{206}Pb ages (Heaman 2009). The U-Pb age of titanite crystals from the Khan pegmatite was investigated first by Kinny *et al.* (1994) using ID-TIMS. Their U-Pb results from six analyses yielded a weighted mean ^{207}Pb/^{206}Pb age of 518 ± 2 Ma (2*s*). Heaman (2009) recommended a weighted mean ^{207}Pb/^{206}Pb age of 522.3 ± 2 Ma (2*s*, *n* = 9, MSWD = 1.0) for nine fractions using TIMS (three aliquots were spiked after dissolution) as the best estimate for the crystallisation age for Khan titanite, whereas the weighted mean ^{206}Pb/^{238}U age of 510.1 ± 4.9 Ma (2*s*, *n* = 10, MSWD = 1.07) was slightly younger and less precise. Chew *et al.* (2014) provided a U-Pb TW concordia intercept age of 520.9 ± 3.9 Ma (2*s*, *n* = 14, MSWD = 4.2) using a Thermo Scientific iCAP-Qc (Q-ICP-MS) coupled to a 193 nm laser system.

The Khan titanite sample used in this study was provided by Larry M. Heaman. Major and trace element compositions are reported in Tables 1 and 3. The mean Fe/Al a.p.f.u. ratio is 0.37

Table 3.
Trace element composition of titanites measured by LA-ICP-MS

Element	Isotope	Unit	Khan (n = 21)		BLR-1 (n = 20)		OLT1 (n = 21)		Ontario (n = 21)		MKED1 (n = 19)		YQ-82 (n = 63)		T3 (n = 21)		T4 (n = 20)		TLS-36 (n = 23)		NW-IOA (n = 20)		Pakistan (n = 22)		C253 (n = 20)	
			Mean	2s	Mean	2s	Mean	2s	Mean	2s	Mean	2s	Mean	2s	Mean	2s	Mean	2s	Mean	2s	Mean	2s	Mean	2s	Mean	2s	Mean	2s
P	31	μg g^{-1}	237	32	103	16	80.2	14.3	100	15	113	62	214	1422							131	54				
Rb	85	μg g^{-1}	< 0.98	–	1.26	0.34	< 0.57	–	1.10	0.29	< 0.56	–	< 2.12	–	2.46	1.86	0.46	0.52	0.31	0.43	1.06	3.66	0.11	0.06	0.11	0.04
Sr	88	μg g^{-1}	23.0	3.7	54.2	2.0	117	9	54.2	2.6	7.99	1.25	9.34	3.35	4.60	0.22	20.13	11.32	76.8	35.4	51.3	8.1	37.0	6.0	33.1	3.8
Y	89	μg g^{-1}	3404	333	3652	96	1230	48	3270	173	947	190	2860	2877	18648	1069	866	1007	1441	538	736	406	645	189	768	70
Zr	92	μg g^{-1}	306	30	830	36	911	30	821	56	111	32	98.5	145.2	230	13	183	121	339	123	351	593	190	35	65.5	3.1
Nb	93	μg g^{-1}	4563	630	3797	120	5690	84	3992	221	747	161	400	307	2271	351	289	181	1612	678	283	248	2110	1099	533	50
Ba	137	μg g^{-1}	< 2.59	–	< 2.96	–	< 2.86	–	< 2.82	–	< 1.51	–	< 2.48	–	0.39	0.94	3.13	12.49	< 0.26	–	< 2.40	–	< 0.12	–	< 0.12	–
La	139	μg g^{-1}	2457	251	403	16	704	14	379	26	509	145	130	84	2148	76	1278	825	3137	716	974	362	97.2	19.1	97.5	10.5
Ce	140	μg g^{-1}	6972	650	1799	70	3021	63	1674	96	2067	583	645	293	7873	283	2766	1062	8377	2706	2443	916	523	114	536	65
Pr	141	μg g^{-1}	845	69	321	8	511	8.6	301	16	339	73	140	67	1257	44	235	129	1033	407	304	113	90	13	100	7
Nd	146	μg g^{-1}	3252	240	1646	35	2404	48	1540	78	1559	258	930	575	5879	250	847	579	4220	1844	1235	514	462	64	550	38
Sm	147	μg g^{-1}	636	43	527	14	498	17	500	25	336	41	412	380	1906	101	139	134	606	261	227	115	133	18	168	9
Eu	153	μg g^{-1}	71.2	4.9	86.0	3.3	104	3	83.1	4.1	63.7	4.5	131	164	128	6	48.9	57.7	146	47	51.4	9.9	25.1	3.3	36.7	1.5
Gd	157	μg g^{-1}	436	33	473	14	283	9	454	21	211	46	424	433	2164	132	119	121	405	161	156	75	115	19	150	9
Tb	159	μg g^{-1}	95.1	7.3	125	4	50.0	2.3	115	5	39.6	4.4	98.4	106.8	485	28	18.8	20.5	53.6	21.5	25.7	14.2	21.2	3.5	26.1	1.8
Dy	163	μg g^{-1}	585	49	873	24	279	11	798	43	218	24	629	694	3444	197	121	135	278	110	137	81	130	26	154	10
Ho	165	μg g^{-1}	118	11	186	6	52.5	2.6	168	9	39.2	4.3	125	134	705	42	24.7	27.5	51.1	19.4	27.2	16.1	24.8	5.4	29.9	1.8
Er	166	μg g^{-1}	340	34	516	16	137	6	466	26	93.4	9.3	317	327	1957	116	79.5	89.0	130	49	73.3	42.6	66.9	17.0	76.7	5.5
Tm	169	μg g^{-1}	53.7	6.2	69.6	2.4	19.0	1.0	62.9	3.3	11.9	1.0	41.8	41.6	284	14	12.1	13.8	18.4	7.0	10.3	6.2	10.0	2.6	10.5	0.8
Yb	172	μg g^{-1}	395	52	379	11	122	6	350	20	67.6	5.3	257	229	1851	94	107	126	127	50	69.3	38.9	68.8	19.3	67.4	5.2
Lu	175	μg g^{-1}	50.1	7.1	30.9	1.1	12.9	0.6	28.8	2.1	6.18	0.70	26.9	19.1	183	9	14.2	16.2	15.9	5.6	7.47	3.90	7.68	2.47	7.27	0.62
Hf	178	μg g^{-1}	39.0	3.2	57.2	3.0	126	6	63.7	5.2	12.3	1.5	10.0	8.3	27.3	1.8	18.6	10.5	37.4	9.8	12.1	23.9	22.4	4.8	6.39	0.47
Ta	181	μg g^{-1}	765	310	174	7	320	8	280	23	42.0	9.5	32.7	55.9	421	57	30.8	30.6	97.7	78.1	3.98	14.2	124	74	187	58
Pb	204	μg g^{-1}	< 5.35	–	< 5.59	–	< 5.54	–	< 5.20	–	< 3.15	–	< 3.44	–	< 2.71	–	< 1.1	–	< 1.64	–	< 4.03	–	< 1.02	–	< 1.08	–
Pb*		μg g^{-1}	70.5	5.8	66.5	3.4	70.3	2.6	55.1	5.5	48.7	11.9	22.4	12.7	63.4	3.2	23.2	25.1	4.25	1.66	6.62	4.55	0.49	0.16	0.31	0.09
Th	232	μg g^{-1}	595	83	219	15	355	14	179	19	321	35	35.6	24.9	281	13	61.5	60.5	418	231	221	333	257	59	214	10
U	238	μg g^{-1}	754	56	334	20	329	13	267	25	106	31	59.8	38.2	296	17	110	127	51.2	18.2	254	198	85.8	29.0	39.3	2.4
REE + Y		μg g^{-1}	19711	1435	11087	267	9427	201	10189	527	6506	1240	7168	6033	48911	2261	6677	2716	20038	6498	6476	2367	2420	419	2779	195
$(La/Lu)_N$			5.28	0.92	1.40	0.05	5.84	0.29	1.41	0.08	8.80	1.98	0.68	1.49	1.26	0.04	14.2	19.5	21.5	5.5	15.7	20.5	1.39	0.50	1.37	0.60
Eu/Eu*			0.41	0.02	0.53	0.01	0.84	0.02	0.53	0.01	0.74	0.09	0.95	0.50	0.19	0.00	1.15	0.39	0.91	0.10	0.88	0.53	0.62	0.04	0.71	0.02

La_N/Lu_N and $Eu/Eu^* = \frac{Eu_N}{\sqrt{(Sm_N \times Gd_N)}}$ were normalised by Boynton (1984). Pb* (μg g^{-1}) = 23.6%*^{206}Pb (μg g^{-1}) + 22.6%*^{207}Pb (μg g^{-1}) + 52.3%*^{208}Pb (μg g^{-1}).

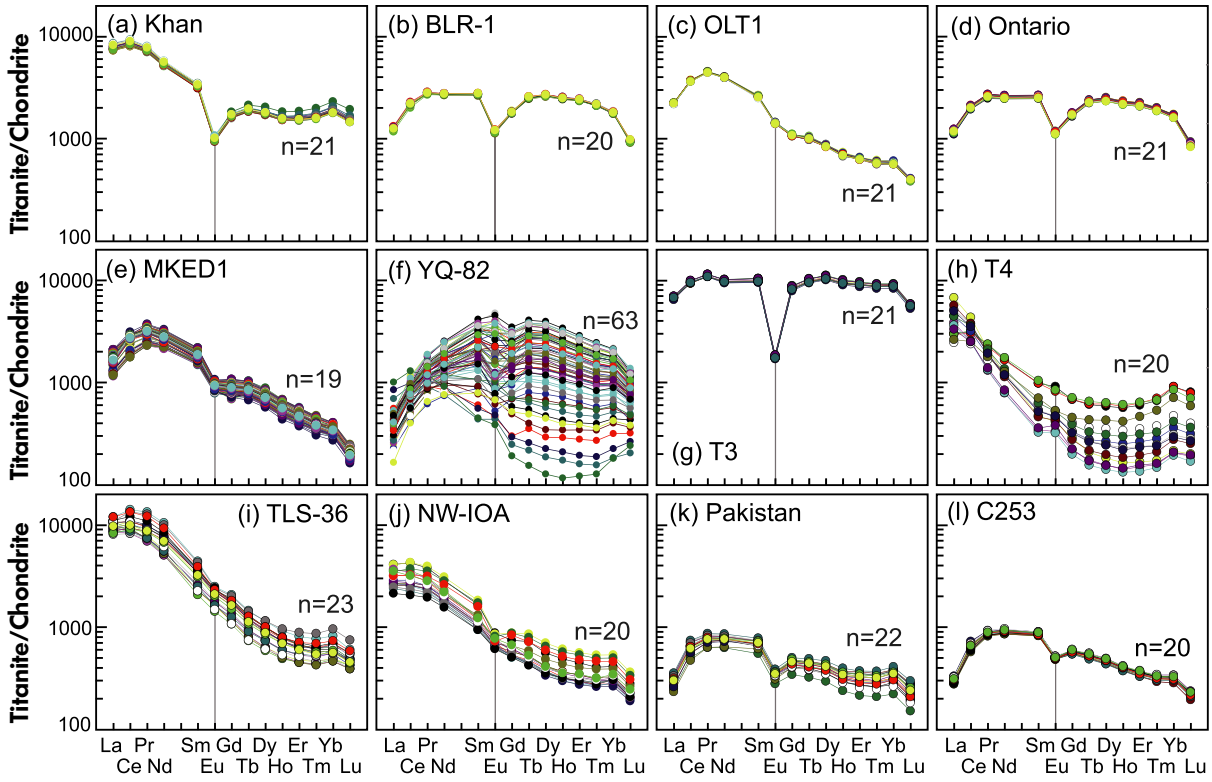

Figure 2. Chondrite-normalised REE patterns for titanites utilised in this study. (a) Khan, (b) BLR-1, (c) OLT1, (d) Ontario, (e) MKED1, (f) YQ-82, (g) T3, (h) T4, (i) TLS-36, (j) NW-IOA, (k) Pakistan and (l) C253. Chondrite-normalised data are from Boynton (1984). [Colour figure can be viewed at wileyonlinelibrary.com]

and plots in the metamorphic field of Kowallis *et al.* (1997). The Khan titanite has high Y (~ 3404 μg g^{-1}), Nb (~ 4563 μg g^{-1}), Ta (~ 765 μg g^{-1}), Nd (~ 3252 μg g^{-1}) and Sm (~ 636 μg g^{-1}) mass fractions. The chondrite-normalised REE pattern is fractionated (mean La/Lu_N = 5.28 ± 0.92) with a strong Eu anomaly (mean Eu/Eu* = 0.41 ± 0.02; Figure 2a).

The U, Th, Pb and Th/U results for the Khan titanite obtained by laser ablation are relatively uniform: 754 ± 56, 595 ± 83, 70 ± 6 and 0.79 ± 0.06 μg g^{-1}, respectively. The measured f_{206} (%) values are generally low and vary between 0.3 and 2.7% with a mean of 0.90 ± 1.28%, reflecting only a small amount of common Pb. The U-Pb results are presented in Table 5 and plotted on a TW diagram, yielding a lower intercept age of 521 ± 3 Ma using an initial Pb composition of 0.87 calculated using the two-stage model of Stacey and Kramers (1975) (Figure 4a). The ^{207}Pb-corrected weighted mean $^{206}Pb/^{238}U$ age is 521 ± 3 Ma (2*s*, *n* = 21). Our U-Pb results from analysis by laser ablation show that Khan has consistent $^{238}U/^{206}Pb$ ratios but relatively variable $^{207}Pb/^{206}Pb$ ratios, reflecting the slightly variable amount of common Pb present in this titanite.

The Khan titanite shows slight variations in $^{147}Sm/^{144}Nd$ and limited variation in $^{143}Nd/^{144}Nd$, ranging from 0.1149 to 0.1278 and from 0.511581 to 0.511694, respectively. All the data points are located along the *ca.* 518 Ma reference isochron (Figure 5a) and yield a mean $\varepsilon_{Nd}(t)$ of -14.3 ± 0.8 (2*s*, *n* = 89; Table 6). Xu *et al.* (2015b) reported a $^{143}Nd/^{144}Nd$ value of 0.511635 ± 0.000028 (2*s*, *n* = 60) using a Neptune Plus MC-ICP-MS and GeoLas 193 nm excimer laser. More recently, the same group reported $^{147}Sm/^{144}Nd$ and $^{143}Nd/^{144}Nd$ values of 0.1217 ± 0.0002 (2*s*, *n* = 77) and 0.511632 ± 0.000030 (2*s*, *n* = 77; Xu *et al.* 2018).

BLR-1

This titanite is commonly used as a U-Pb reference material for SIMS and LA-ICP-MS analyses (Bonamici *et al.* 2015). It is a metamorphic megacryst collected from Bear Lake Diggings near Tory Hill, Ontario, Canada (Mazdab 2009). Six individual BLR-1 fragments were dated by ID-TIMS (three were abraded for 3 h in an alumina-ceramic vertical abrader to form smooth ellipsoids, and three were unabraded), and five fragments yielded a weighted mean $^{206}Pb/^{238}U$ age of 1047.1 ±

Table 4.
Sm and Nd mass fractions and $^{147}Sm/^{144}Nd$ and $^{143}Nd/^{144}Nd$ isotopic ratios of titanites and international certified reference materials measured by ID-MC-ICP-MS in this study

Titanite	Sm (μg g^{-1})	Nd (μg g^{-1})	$^{147}Sm/^{144}Nd$	$^{143}Nd/^{144}Nd$	2SE	$^{143}Nd/^{144}Nd$ (t)	$\varepsilon_{Nd}(t)$
BLR-1 (~ 1047 Ma)							
1_01	439	1381	0.1921	0.512815	0.000004	0.511495	4.07
1_02	439	1381	0.1921	0.512813	0.000015	0.511493	4.04
1_03	439	1381	0.1922	0.512816	0.000009	0.511496	4.09
Ontario (~ 1053 Ma)							
1	491	1534	0.1936	0.512829	0.000007	0.511491	4.15
2	477	1501	0.1923	0.512835	0.000010	0.511506	4.45
3	502	1577	0.1925	0.512830	0.000009	0.511500	4.32
4	501	1571	0.1926	0.512837	0.000010	0.511506	4.44
Mean	493	1546	0.1928	0.512833		0.511501	4.34
2*s*	23	71	0.0011	0.000008		0.000014	0.28
T3 (~ 1130 Ma)							
1	1805	5578	0.1957	0.512608	0.000010	0.511157	-0.43
2	1923	5957	0.1952	0.512605	0.000008	0.511157	-0.43
3	1902	5867	0.1960	0.512614	0.000007	0.511160	-0.37
4	1905	5868	0.1962	0.512618	0.000007	0.511163	-0.32
Mean	1884	5817	0.1958	0.512611		0.511159	-0.39
2*s*	106	331	0.0009	0.000012		0.000006	0.11
T4 (~ 1130 Ma)							
1	96	628	0.0924	0.511846	0.000008	0.511161	-0.36
TLS-36 (~ 135 Ma)							
1	517	3024	0.1033	0.512263	0.000010	0.512172	-5.71
2	520	3043	0.1033	0.512271	0.000009	0.512180	-5.55
3	501	2906	0.1042	0.512273	0.000009	0.512181	-5.52
4	487	2917	0.1009	0.512273	0.000007	0.512184	-5.47
Mean	506	2973	0.1029	0.512270		0.512179	-5.56
2*s*	31	142	0.0029	0.000010		0.000011	0.21
NW-IOA (~ 130 Ma)							
1	316	1738	0.1100	0.512143	0.000009	0.512049	-8.22
Pakistan (~ 21 Ma)							
1	159	541	0.1777	0.512164	0.000012	0.512141	-9.20
2	207	699	0.1790	0.512153	0.000007	0.512130	-9.41
3	154	526	0.1764	0.512136	0.000007	0.512113	-9.75
4	161	551	0.1765	0.512142	0.000007	0.512119	-9.62
Mean	170	579	0.1774	0.512149		0.512126	-9.49
2*s*	49	160	0.0025	0.000025		0.000025	0.48
C253 (~ 20 Ma)							
1	212	703	0.1824	0.512146	0.000011	0.512122	-9.56
2	210	692	0.1832	0.512135	0.000009	0.512111	-9.78
3	196	642	0.1845	0.512133	0.000012	0.512109	-9.81
4	196	644	0.1839	0.512138	0.000008	0.512114	-9.72
Mean	203	670	0.1835	0.512138		0.512114	-9.72
2*s*	17	64	0.0018	0.000011		0.000012	0.23

0.4 Ma (2*s*, MSWD = 0.56). The sixth (unabraded) fragment, with a slightly hackly texture on the surface, exhibited a younger age, indicating that it was originally adjacent to a fracture and had a minor amount of Pb loss near the surface (Aleinikoff *et al.* 2007). In addition, Sun *et al.* (2012) reported ^{207}Pb-corrected weighted mean $^{206}Pb/^{238}U$ ages of 1046 ± 5 Ma (2*s*, n = 24) and 1046 ± 6 Ma (2*s*, n = 24) using single spot and line raster scan analyses, respectively.

Table 4 (continued).

CRMs	Sm (μg g^{-1})		Nd (μg g^{-1})		$^{147}Sm/^{144}Nd$		$^{143}Nd/^{144}Nd$		
	This study	Ref. value	This study	Ref. value	This study	Ref. value	This study	2SE	Ref. value
BCR-2									
1	6.37	6.54 [b]	28.09	28.60 [b]	0.1370	0.1383 [b]	0.512635	0.000007	0.512637 [a]
2	6.40	6.51 [c]	28.19	28.43 [c]	0.1373	0.1385 [c]	0.512643	0.000006	0.512641 [b]
3	6.50		28.36		0.1386		0.512642	0.000008	0.512637 [c]
Mean	6.42		28.21		0.1376		0.512640		
2*s*	0.14		0.27		0.0017		0.000009		
AGV-2									
1	5.47	5.50 [b]	30.34	30.47 [b]	0.1089	0.1092 [b]	0.512781	0.000013	0.512791 [a]
2	5.43	5.44 [c]	30.16	30.25 [c]	0.1089	0.1098 [c]	0.512788	0.000019	0.512811 [b]
Mean	5.45		30.25		0.1089		0.512785		0.512789 [c]
2*s*	0.05		0.25		0.0001		0.000011		

Reference values for CRMs are from [a] Weis *et al.* (2006), [b] Chu *et al.* (2009) and [c] Yang *et al.* (2011).

The studied BLR-1 titanite crystal was offered by John N. Aleinikoff. The crystal is dark brown to black in colour. BSE images were taken of a number of fragments from this titanite and most are relatively uniform and lack mineral inclusions (Figure 1b). The homogeneous nature of the crystal is supported by the narrow range in major and trace element compositions (Tables 1 and 3). BLR-1 has high Y (3652 ± 96 μg g^{-1}), Zr (830 ± 36 μg g^{-1}), Nb (3797 ± 120 μg g^{-1}) and LREE mass fractions. The chondrite-normalised REE pattern is flat for the MREE (except for Eu). The Eu anomaly (Eu/Eu*) is 0.53 ± 0.01, showing what has been described as a 'seagull' pattern (Figure 2b), similar to that reported by Aleinikoff *et al.* (2007).

The mean U, Th and Pb mass fractions for BLR-1 are 334 ± 20, 219 ± 15 and 67 ± 3 μg g^{-1}, respectively. The mean Th/U ratio is 0.65 ± 0.01. The U-Pb results are plotted on a TW diagram, yielding a lower intercept age of 1048 ± 7 Ma (2*s*, *n* = 20; Figure 4b) and a ^{207}Pb-corrected weighted mean $^{206}Pb/^{238}U$ age of 1048 ± 7 Ma (2*s*, *n* = 20).

The Sm and Nd mass fractions of 439 and 1381 μg g^{-1}, respectively, were given by the solution method (Table 4). Laser ablation analysis of BLR-1 yielded mean $^{147}Sm/^{144}Nd$ values of 0.1939 ± 0.0045 and a $^{143}Nd/^{144}Nd$ ratio of 0.512829 ± 0.000047 (*n* = 175, 2*s*) (Table 6), somewhat higher than, but still in agreement (within uncertainty) with the solution values of $^{147}Sm/^{144}Nd$ of 0.1921 and $^{143}Nd/^{144}Nd$ ratio of 0.512815 ± 0.000004 (*n* = 1, 2SE; Figure 6a, b). More recently, Xu *et al.* (2018) reported $^{147}Sm/^{144}Nd$ and $^{143}Nd/^{144}Nd$ values of 0.1982 ± 0.0048 (2*s*, *n* = 45) and 0.512818 ± 0.000082 (2*s*, *n* = 45) using LA-MC-ICP-MS.

OLT1

Titanite OLT1, sampled at Otter Lake, Quebec, within the Grenville Province of the Canadian Shield, is a dark reddish brown single crystal from a large metasomatic calcite skarn at the Yates uranium prospect, where the rocks are rich in augite, scapolite and titanite. It has a concordant ID-TIMS age of 1014.8 ± 2.0 Ma (2*s*, *n* = 6, MSWD = 1.8; Kennedy *et al.* 2010). Detailed SEM, Raman, EBSD, EPMA-WDS and SIMS U-Th-Pb dating showed the potential of OLT1 as a reference material for *in situ* U-Pb dating, with only limited U-Pb age heterogeneity (Kennedy *et al.* 2010). Sun *et al.* (2012) reported a ^{207}Pb-corrected weighted mean $^{206}Pb/^{238}U$ ages of 1015 ± 5 Ma (2*s*, *n* = 24) and 1017 ± 6 Ma (2*s*, *n* = 24) using single spot and line raster scan modes, respectively, using BLR-1 as the calibrating reference material. Xu *et al.* (2015b) reported a $^{143}Nd/^{144}Nd$ value of 0.512270 ± 0.000024 (2*s*, *n* = 64) using a Neptune Plus MC-ICP-MS and GeoLas 193 nm excimer laser. $^{147}Sm/^{144}Nd$ and $^{143}Nd/^{144}Nd$ values of 0.1313 ± 0.0019 (2*s*, *n* = 107) and 0.512270 ± 0.000026 (2*s*, *n* = 107), respectively, were also reported by the same group (Xu *et al.* 2018).

The studied OLT1 material was provided by Allen K. Kennedy. It has high Y (1230 ± 48 μg g^{-1}), Zr (911 ± 30 μg g^{-1}), Nb (5690 ± 84 μg g^{-1}), Nd (2404 ± 48 μg g^{-1}) and Sm (~ 498 ± 17 μg g^{-1}) mass fractions (Table 3). The chondrite-normalised REE patterns for all analyses are identical with LREE/HREE fractionation (La/Lu_N = 5.84 ± 0.29), and slightly negative europium anomalies (Eu/Eu* = 0.84 ± 0.02; Figure 2c).

The OLT1 U-Pb dating results are presented in Table 5 and on a TW concordia diagram in Figure 4c. The U, Th and

Table 5.
Compilation of titanite U-Pb dating results by LA-ICP-MS in this study

Titanite	*n*	Pb (μg g^{-1}) (2*s*)	Th (μg g^{-1}) (2*s*)	U (μg g^{-1}) (2*s*)	Th/U (2*s*)	$^{238}U/^{206}Pb$		$^{207}Pb/^{206}Pb$		$^{207}Pb/^{235}U$		$^{206}Pb/^{238}U$		$^{208}Pb/^{232}Th$		f_{206} (%) [a]		f_{208} (%) [b]		^{207}Pb Corr. Age (Ma)		Reference age [c]
						Mean	2*s*	Mean	2*s*	Mean	2*s*	Mean	2*s*	Mean	2*s*	Mean	2*s*	Mean	2*s*	Mean	2*s*	
Khan	21	70 (6)	595 (83)	754 (56)	0.79 (0.06)	11.78	0.27	0.0651	0.0104	0.76	0.13	0.0849	0.0020	0.0281	0.0030	0.90	1.28	7.30	10.32	521	3	518 ± 2 Ma[1]; 522.3 ± 2.0 Ma[2]
BLR-1	20	67 (3)	219 (15)	334 (20)	0.65 (0.01)	5.58	0.07	0.0861	0.0025	2.13	0.07	0.1791	0.0023	0.0617	0.0018	1.42	0.29	13.0	28.8	1048	7	1047.1 ± 0.4 Ma[3]
OLT1	21	70 (3)	355 (14)	329 (13)	1.08 (0.02)	5.81	0.08	0.0833	0.0034	1.98	0.09	0.1720	0.0025	0.0551	0.0023	1.23	0.41	8.70	7.34	1011	6	1014.8 ± 2.0 Ma[4]
Ontario	21	55 (6)	179 (19)	267 (25)	0.67 (0.03)	5.57	0.11	0.0892	0.0026	2.21	0.06	0.1796	0.0035	0.0629	0.0025	1.77	0.31	22.1	22.5	1047	6	1053.3 ± 3.1 Ma[5]
MKED1	19	49 (12)	321 (35)	106 (31)	3.07 (0.87)	3.76	0.13	0.0943	0.0017	3.46	0.10	0.2659	0.0090	0.0766	0.0043	0.07	0.20	0.64	2.39	1516	10	1521.02 ± 0.55 Ma[6]
YQ-82	63	22 (13)	36 (25)	60 (38)	0.67 (0.84)	3.06	0.20	0.1126	0.0028	5.08	0.37	0.3276	0.0215	0.0977	0.0082	0.01	0.32	11.7	20.0	1840	11	1837.6 ± 1.0 Ma[7]
T3	21	63 (3)	281 (13)	296 (17)	0.95 (0.07)	5.16	0.15	0.0772	0.0024	2.06	0.11	0.1938	0.0058	0.0572	0.0035	-0.02	0.28	2.49	10.7	1125	14	
T4	20	23 (25)	62 (61)	110 (127)	0.58 (0.17)	5.21	0.19	0.0794	0.0044	2.10	0.15	0.1921	0.0070	0.0604	0.0073	0.25	0.54	-35.5	329	1131	8	
TLS-36	23	4.2 (1.7)	418 (231)	51 (18)	8.08 (2.10)	38.73	3.77	0.1891	0.0542	0.68	0.26	0.0259	0.0026	0.0084	0.0015	17.6	6.8	13.8	5.8	135	2	136.0 ± 1.5 Ma[8]
NW-IOA	20	6.6 (4.6)	221 (333)	254 (198)	0.93 (1.37)	48.51	1.98	0.0573	0.0152	0.16	0.05	0.0206	0.0009	0.0071	0.0027	1.06	1.92	7.06	74.45	130	1	129.7 ± 0.8 Ma[9]
Pakistan	22	0.49 (0.16)	257 (59)	86 (29)	3.07 (1.10)	297.5	23.3	0.0550	0.0213	0.03	0.01	0.0034	0.0003	0.0011	0.0004	1.08	2.70	3.07	11.15	21.4	0.4	
C253	20	0.31 (0.09)	214 (10)	39 (2)	5.45 (0.44)	304.0	27.6	0.1100	0.0463	0.05	0.02	0.0033	0.0003	0.0010	0.0005	8.04	5.86	12.2	18.2	19.5	0.4	

[a] f_{206}, common ^{206}Pb in total ^{206}Pb; $f_{206} = \frac{\left(^{207}Pb/^{206}Pb\right)_{Meas} - \left(^{207}Pb/^{206}Pb\right)^{*}}{\left(^{207}Pb/^{206}Pb\right)_{Comm} - \left(^{207}Pb/^{206}Pb\right)^{*}}$;

[b] f_{208}, common ^{208}Pb in total ^{208}Pb; $f_{208} = \frac{\left(^{207}Pb/^{208}Pb\right)_{Meas} - \left(^{207}Pb/^{208}Pb\right)^{*}}{\left(^{207}Pb/^{208}Pb\right)_{Comm} - \left(^{207}Pb/^{208}Pb\right)^{*}}$.

[c] Reference ages: 1, ID-TIMS $^{207}Pb/^{206}Pb$ age from Kinny *et al.* (1994); 2, TIMS $^{207}Pb/^{206}Pb$ age from Heaman (2009); 3, ID-TIMS $^{206}Pb/^{238}U$ age from Aleinikoff *et al.* (2007); 4, concordant ID-TIMS age from Kennedy *et al.* (2010); 5, ID-TIMS $^{206}Pb/^{238}U$ age from Spencer *et al.* (2013); 6, ID-TIMS $^{207}Pb/^{206}Pb$ age from Spandler *et al.* (2016); 7, ID-TIMS $^{206}Pb/^{238}U$ age from Huyskens *et al.* (2016); 8, laser ablation $^{206}Pb/^{238}U$ age from Li *et al.* (2010); 9, laser ablation ^{207}Pb-corrected $^{206}Pb/^{238}U$ age from Liu *et al.* (2018).

Table 6.
Sm-Nd isotopic data of titanite using LA-MC-ICP-MS in this study

Titanite	*n*	$[^{147}Sm/^{144}Nd]_m$ (± 2*s*)	2RSD (%)	$[^{143}Nd/^{144}Nd]_m$ (± 2*s*)	$^{143}Nd/^{144}Nd(t)$ (± 2*s*)	$[^{145}Nd/^{144}Nd]_m$ (± 2*s*)	$\varepsilon_{Nd}(t)$ (± 2*s*)	'External' RM
Khan (~ 518 Ma)								
2016.09.05	20	0.1186 (68)	5.7	0.511627 (43)	0.511225 (38)	0.348426 (26)	-14.6 (0.7)	MKED1
2017.02.24	9	0.1178 (28)	2.4	0.511645 (38)	0.511246 (46)	0.348431 (45)	-14.2 (0.9)	MKED1
2018.05.12	20	0.1181 (31)	2.6	0.511644 (30)	0.511243 (32)	0.348443 (28)	-14.2 (0.6)	Ontario
2018.05.13	20	0.1191 (29)	2.4	0.511645 (33)	0.511241 (33)	0.348436 (26)	-14.3 (0.7)	BLR-1
2018.05.14	20	0.1199 (63)	5.2	0.511642 (41)	0.511238 (39)	0.348434 (30)	-14.2 (0.7)	Ontario
Mean	89	0.1188 (50)	4.2	0.511642 (41)	0.511238 (39)	0.348427 (33)	-14.3 (0.8)	
BLR-1 (~ 1047 Ma)								
2010.12.30	20	0.1961 (28)	1.4	0.512837 (35)	0.511489 (33)	0.348433 (18)	3.97 (0.64)	Ontario
2016.09.05	40	0.1932 (37)	1.9	0.512821 (50)	0.511493 (42)	0.348421 (21)	4.05 (0.82)	MKED1
2016.09.13	22	0.1937 (16)	0.8	0.512804 (29)	0.511473 (26)	0.348421 (27)	3.92 (0.77)	OLT1
2017.02.25	9	0.1939 (68)	3.5	0.512825 (37)	0.511492 (37)	0.348421 (31)	3.92 (0.77)	MKED1
2017.03.04	28	0.1947 (44)	2.2	0.512823 (31)	0.511485 (42)	0.348411 (34)	3.88 (0.81)	Ontario
2018.05.12	31	0.1927 (58)	3.0	0.512841 (33)	0.511517 (48)	0.348429 (28)	4.52 (0.94)	Ontario
2018.05.14	25	0.1943 (29)	1.5	0.512848 (43)	0.511513 (38)	0.348437 (29)	4.43 (0.74)	Ontario
Mean	175	0.1939 (45)	2.3	0.512829 (47)	0.511496 (49)	0.348424 (31)	4.10 (0.96)	
OLT1 (~ 1015 Ma)								
2010.12.30	31	0.1234 (11)	0.9	0.512201 (29)	0.511380 (27)	0.348429 (18)	1.01 (0.53)	Ontario
2016.09.06	40	0.1240 (12)	1.0	0.512206 (30)	0.511380 (28)	0.348425 (18)	1.02 (0.55)	MKED1
2016.09.07	10	0.1243 (10)	0.8	0.512205 (23)	0.511378 (24)	0.348425 (20)	0.97 (0.47)	Ontario
2016.09.13	21	0.1231 (11)	0.9	0.512207 (33)	0.511387 (36)	0.348421 (26)	1.16 (0.69)	BLR-1
2017.02.25	10	0.1253 (20)	1.6	0.512210 (38)	0.511375 (43)	0.348424 (34)	0.92 (0.84)	MKED1
2017.03.04	21	0.1243 (12)	1.0	0.512212 (37)	0.511384 (31)	0.348413 (29)	1.09 (0.60)	Ontario
2018.05.12	15	0.1232 (35)	2.8	0.512224 (37)	0.511403 (44)	0.348438 (29)	1.47 (0.86)	Ontario
2018.05.13	36	0.1232 (17)	1.4	0.512237 (36)	0.511417 (35)	0.348440 (19)	1.74 (0.68)	BLR-1
Mean	184	0.1237 (20)	1.6	0.512214 (41)	0.511390 (44)	0.348428 (28)	1.21 (0.86)	
Ontario (~ 1053 Ma)								
2010.12.30	31	0.1937 (10)	0.5	0.512812 (27)	0.511473 (26)	0.348432 (23)	3.80 (0.51)	OLT1
2017.09.05	20	0.1908 (27)	1.4	0.512808 (39)	0.511489 (34)	0.348427 (23)	4.12 (0.66)	MKED1
2017.09.06	20	0.1901 (13)	0.7	0.512806 (35)	0.511492 (33)	0.348419 (21)	4.19 (0.64)	MKED1
2017.09.07	10	0.1900 (10)	0.5	0.512802 (39)	0.511488 (37)	0.348420 (42)	4.11 (0.72)	MKED1
2017.09.23	9	0.1914 (15)	0.8	0.512821 (37)	0.511498 (36)	0.348384 (60)	4.29 (0.70)	OLT1
2017.03.04	21	0.1923 (25)	1.3	0.512812 (31)	0.511483 (30)	0.348419 (41)	4.00 (0.58)	OLT1
2018.05.13	34	0.1913 (25)	1.3	0.512832 (34)	0.511509 (33)	0.348433 (23)	4.52 (0.64)	BLR-1
Mean	145	0.1916 (32)	1.7	0.512815 (41)	0.511490 (40)	0.348424 (39)	4.15 (0.79)	
MKED1 (~ 1521 Ma)								
2016.09.05	25	0.1255 (28)	2.2	0.511636 (58)	0.510353 (57)	0.348430 (17)	-6.24 (1.11)	Ontario
2016.09.06	4	0.1288 (17)	1.3	0.511625 (32)	0.510338 (23)	0.348430 (22)	-6.53 (0.45)	Ontario
2018.05.12	20	0.1289 (23)	1.8	0.511651 (20)	0.510363 (29)	0.348440 (28)	-6.05 (0.57)	Ontario
2018.05.14	15	0.1286 (30)	2.4	0.511644 (28)	0.510358 (42)	0.348434 (18)	-6.14 (0.83)	Ontario
Mean	64	0.1286 (27)	2.1	0.511642 (43)	0.510356 (45)	0.348434 (23)	-6.17 (0.89)	
YQ-82 (~ 1838 Ma)								
2016.09.06	15	0.2647 (655)	25	0.513270 (778)	0.510070 (69)	0.348433 (35)	-3.73 (1.36)	MKED1
2018.05.13	13	0.2452 (1149)	47	0.513020 (1380)	0.510055 (81)	0.348445 (30)	-4.02 (1.58)	BLR-1
Mean	28	0.2556 (921)	36	0.513154 (1106)	0.510063 (75)	0.348438 (34)	-3.86 (1.47)	
T3 (~ 1130 Ma)								
2018.05.12	9	0.1967 (18)	0.9	0.512620 (34)	0.511161 (30)	0.348444 (37)	-0.35 (0.59)	Ontario
2018.05.13	9	0.1978 (20)	1.0	0.512644 (22)	0.511177 (21)	0.348439 (22)	-0.04 (0.41)	BLR-1
2018.05.14	19	0.1988 (21)	1.1	0.512642 (29)	0.510906 (35)	0.348441 (29)	-0.27 (0.68)	Ontario
Mean	37	0.1980 (26)	1.3	0.512637 (35)	0.511169 (31)	0.348441 (29)	-0.20 (0.61)	
T4 (~ 1130 Ma)								
2018.05.12	30	0.0965 (321)	33	0.511884 (225)	0.511168 (63)	0.348425 (28)	-0.22 (1.24)	Ontario
2018.05.13	30	0.1021 (371)	36	0.511934 (276)	0.511177 (55)	0.348432 (32)	-0.04 (1.07)	BLR-1
2018.05.14	15	0.0921 (235)	26	0.511867 (151)	0.511183 (63)	0.348431 (47)	0.08 (1.24)	Ontario
Mean	75	0.0979 (333)	34	0.511901 (239)	0.511174 (60)	0.348429 (34)	-0.09 (1.18)	

Pb mass fractions are relatively uniform: 329 ± 13, 355 ± 14 and 70 ± 3 μg g^{-1}, respectively. OLT1 has a uniform Th/U ratio of 1.08 ± 0.02 and contains a relatively low proportion of f_{206} (%) (1.23 ± 0.41) and relatively high f_{208} (%) (8.7 ± 7.3). Thus, the OLT1 U-Pb age is more useful than its Th-Pb age. All twenty-one ages are clustered near the

Table 6 (continued).
Sm-Nd isotopic data of titanite using LA-MC-ICP-MS in this study

Titanite	*n*	$[^{147}Sm/^{144}Nd]_m$ (± 2*s*)	2RSD (%)	$[^{143}Nd/^{144}Nd]_m$ (± 2*s*)	$^{143}Nd/^{144}Nd(t)$ (± 2*s*)	$[^{145}Nd/^{144}Nd]_m$ (± 2*s*)	$\varepsilon_{Nd}(t)$ (± 2*s*)	'External' RM
TLS-36 (~ 135 Ma)								
2016.09.06	20	0.1034 (105)	10	0.512241 (54)	0.512150 (53)	0.348425 (24)	-6.13 (1.03)	MKED1
2018.05.12	20	0.1011 (126)	12	0.512273 (36)	0.512183 (36)	0.348440 (19)	-5.48 (0.71)	Ontario
2018.05.13	20	0.1031 (127)	12	0.512273 (61)	0.512182 (59)	0.348432 (32)	-5.50 (1.14)	BLR-1
2018.05.14	20	0.1051 (133)	13	0.512275 (63)	0.512182 (63)	0.348437 (36)	-5.51 (1.23)	Ontario
Mean	80	0.1032 (124)	12	0.512265 (60)	0.512174 (60)	0.348434 (30)	-5.66 (1.17)	
NW-IOA (~ 130 Ma)								
2016.09.06	20	0.1074 (57)	5.3	0.512122 (34)	0.512031 (34)	0.348419 (28)	-8.59 (0.66)	MKED1
2018.05.12	20	0.1082 (78)	7.2	0.512150 (50)	0.512058 (47)	0.348433 (26)	-8.06 (0.91)	Ontario
2018.05.13	20	0.1095 (93)	8.5	0.512161 (41)	0.512067 (43)	0.348438 (28)	-7.87 (0.84)	BLR-1
2018.05.14	20	0.1108 (105)	9.5	0.512156 (61)	0.512062 (59)	0.348441 (38)	-7.98 (1.15)	Ontario
Mean	80	0.1090 (88)	8.1	0.512147 (56)	0.512054 (54)	0.348433 (34)	-8.12 (1.05)	
Pakistan (~ 21 Ma)								
2016.09.06	20	0.1765 (105)	5.9	0.512123 (73)	0.512100 (72)	0.348429 (34)	-9.99 (1.41)	MKED1
2018.05.12	20	0.1721 (80)	4.7	0.512138 (53)	0.512116 (53)	0.348425 (38)	-9.68 (1.03)	Ontario
2018.05.13	20	0.1754 (110)	6.3	0.512134 (83)	0.512111 (83)	0.348422 (36)	-9.78 (1.61)	BLR-1
2018.05.14	20	0.1783 (97)	5.4	0.512152 (53)	0.512128 (53)	0.348438 (29)	-9.44 (1.04)	Ontario
Mean	80	0.1756 (107)	6.1	0.512137 (69)	0.512114 (68)	0.348429 (36)	-9.72 (1.33)	
C253 (~ 20 Ma)								
2017.02.25	12	0.1789 (35)	2.0	0.512148 (97)	0.512125 (97)	0.348436 (104)	-9.51 (1.89)	BLR-1
2018.05.12	20	0.1850 (115)	6.2	0.512139 (60)	0.512115 (60)	0.348427 (26)	-9.70 (1.18)	Ontario
2018.05.13	20	0.1891 (83)	4.4	0.512148 (57)	0.512124 (57)	0.348432 (37)	-9.53 (1.12)	BLR-1
2018.05.14	12	0.1878 (78)	4.2	0.512153 (77)	0.512129 (78)	0.348448 (35)	-9.43 (1.51)	Ontario
Mean	64	0.1857 (113)	6.1	0.512146 (70)	0.512122 (70)	0.348434 (54)	-9.56 (1.36)	

$\varepsilon_{Nd}(t) = \left[\frac{\left(^{143}Nd/^{144}Nd_{Sample}\right) - \left(^{147}Sm/^{144}Nd_{Sample}\right)\times\left(e^{\lambda t}-1\right)}{\left(^{143}Nd/^{144}Nd_{CHUR}\right) - \left(^{147}Sm/^{144}Nd_{CHUR}\right)\times\left(e^{\lambda t}-1\right)} - 1\right] \times 10^4$; $\lambda = 6.54 \times 10^{-12} y^{-1}$ (Lugmair and Marti 1978); $(^{147}Sm/^{144}Nd)_{CHUR} = 0.1967$, and $(^{143}Nd/^{144}Nd)_{CHUR} = 0.512638$ (Jacobsen and Wasserburg 1980).

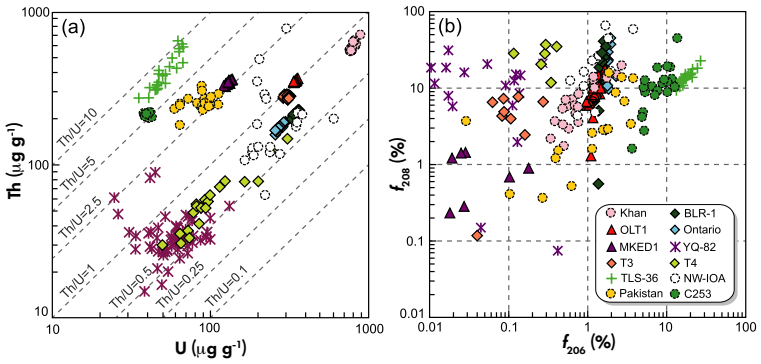

Figure 3. Plots of (a) U versus Th (µg g^{-1}) and (b) f_{206} versus f_{208} of titanites investigated in this study. f_{206} and f_{208} represent common ^{206}Pb in proportion to total ^{206}Pb and common ^{208}Pb in proportion to total ^{208}Pb, respectively. Formulas of f_{206} and f_{208} are available in Table 5. [Colour figure can be viewed at wileyonlinelibrary.com]

concordia, yielding a lower intercept age of 1011 ± 6 Ma (2*s*), consistent with the ^{207}Pb-corrected weighted mean $^{206}Pb/^{238}U$ age of 1011 ± 6 Ma (2*s*).

Long-term Sm-Nd measurements (laser ablation) yielded mean $^{147}Sm/^{144}Nd$ and $^{143}Nd/^{144}Nd$ ratios of 0.1237 ± 0.0020 and 0.512214 ± 0.000041 (*n* = 184, 2*s*), respectively (Table 6, Figure 6c, d). Notably, the $^{147}Sm/^{144}Nd$ values show only minor variation (RSD < 1%), indicating OLT1 is a potential reference material for *in situ* $^{147}Sm/^{144}Nd$ determination. The mean $^{145}Nd/^{144}Nd$ ratio of 0.348428 ± 0.000028 (*n* = 184, 2*s*) is in close agreement with the recommended value of 0.348415. Due to limited supply in this study, OLT1 was not analysed by solution methods.

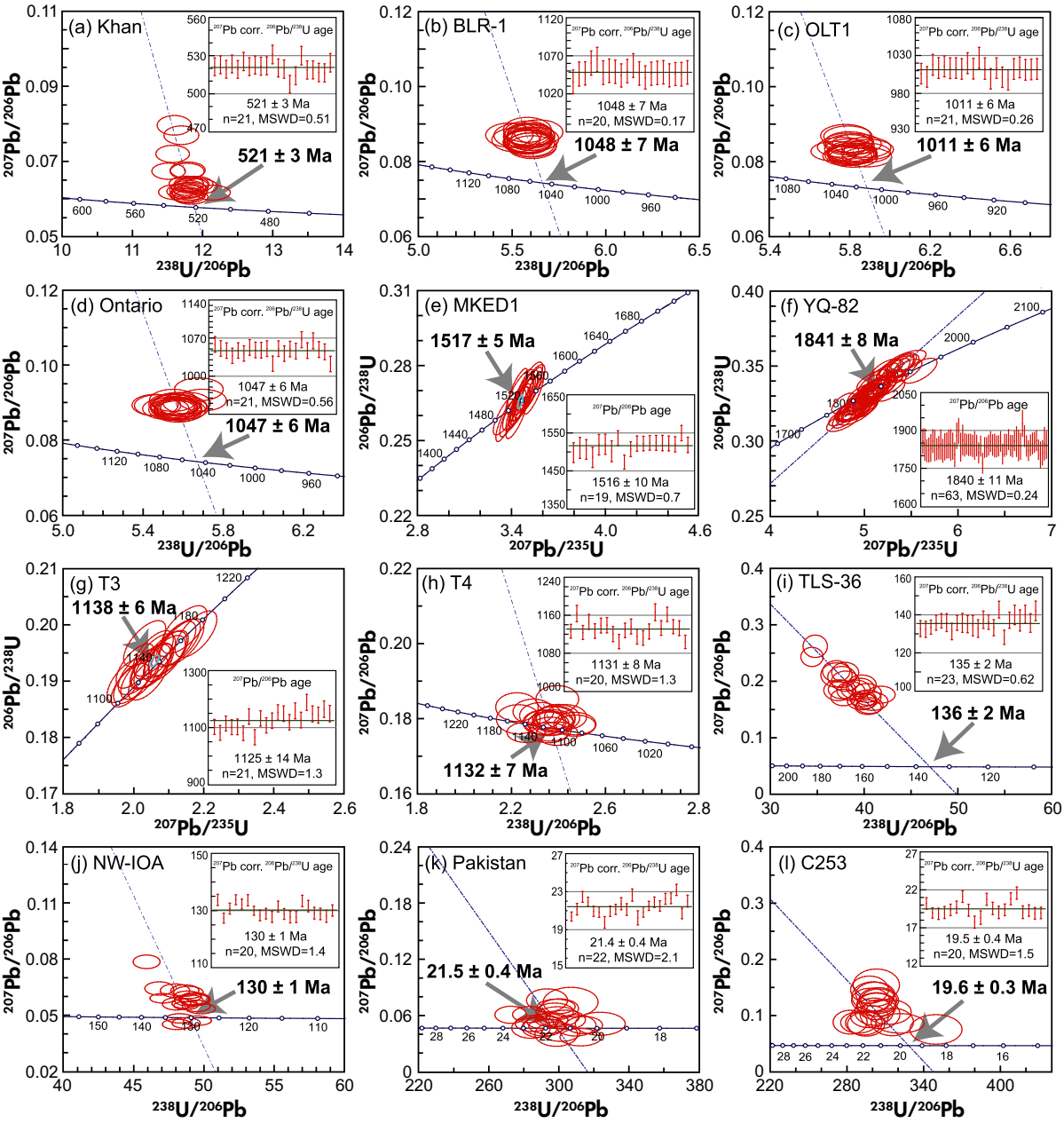

Figure 4. Diagrams of U-Pb dating results for studied titanites. Results of (a) Khan, (b) BLR-1, (c) OLT1, (d) Ontario, (h) T4, (i) TLS-36, (j) NW-IOA, (k) Pakistan and (l) C253 are displayed on Tera–Wasserburg diagram, and the weighted mean $^{206}Pb/^{238}U$ ages are after ^{207}Pb correction. Results of (e) MKED1, (f) YQ-82 and (g) T3 are displayed on concordia diagram, and the weighted mean $^{207}Pb/^{206}Pb$ ages are calculated based on their $^{207}Pb/^{206}Pb$ apparent ages. [Colour figure can be viewed at wileyonlinelibrary.com]

Ontario

This titanite is a dark brown single crystal sampled from the Renfrew district of Ontario, Canada. The crystal size in this study was about 2.5 × 1.5 cm. A detailed LA-ICP-MS analysis of Ontario titanite was conducted by Sun *et al.* (2012), yielding a weighted mean $^{206}Pb/^{238}U$ age of 1056 ± 5 Ma (2*s*, *n* = 28) after ^{207}Pb correction, using BLR-1 as the calibrating reference material. This result was further confirmed by an ID-TIMS $^{206}Pb/^{238}U$ age of 1053.3 ± 3.1 Ma (± 95% C.I., *n* = 6; Spencer *et al.* 2013). This group also obtained a $^{206}Pb/^{238}U$–$^{207}Pb/^{206}Pb$ isochron age of 1048.7 ± 2.6 Ma using a Photon Machines 193 nm ArF excimer laser coupled to a Nu Instruments

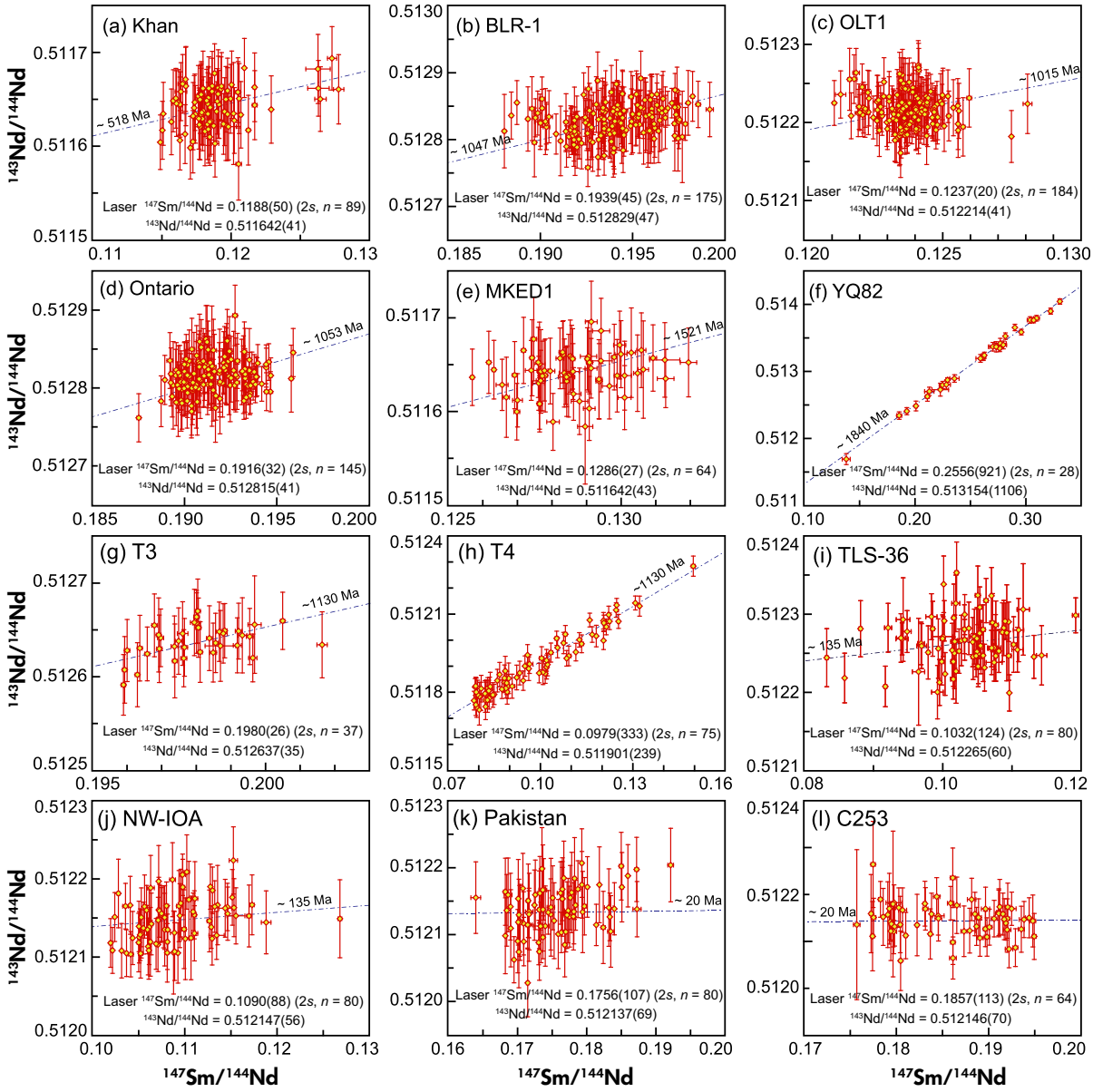

Figure 5. Diagrams of Sm-Nd isotopic values for studied titanites. (a) Khan, (b) BLR-1, (c) OLT1, (d) Ontario, (e) MKED1, (f) YQ-82, (g) T3, (h) T4, (i) TLS-36, (j) NW-IOA, (k) Pakistan and (l) C253. [Colour figure can be viewed at wile yonlinelibrary.com]

Plasma high-resolution MC-ICP-MS. Horstwood *et al.* (2016) recalculated the age uncertainty based on these TIMS data using an improved uncertainty propagation protocol, identifying random and systematic components, which yielded a $^{206}Pb/^{238}U$ age of 1053.5 ± 5.9 Ma.

The fragments of the Ontario titanite are typically homogeneous in BSE images, but mineral inclusions have been discovered, including mm-scale fluorite and magnetite at the μm scale (Figure 1d). The major and trace element compositions are shown in Tables 1 and 3. The Fe/Al a.p.f.u. ratio is 0.68 and falls in the metamorphic field of Kowallis *et al.* (1997). The Ontario titanite contains abundant Y (3270 ± 173 μg g^{-1}), Zr (821 ± 56 μg g^{-1}), Nb (3992 ± 221 μg g^{-1}) and REEs. The chondrite-normalised REE pattern is somewhat fractionated (mean La/Lu_N = 1.41 ± 0.08) with a relatively pronounced Eu anomaly (Eu/Eu* = 0.53 ± 0.01), similar to BLR-1 (Figure 2d). A significant M-type lanthanide tetrad effect is observed in Ontario titanite. Tetrad REE patterns are generally developed in titanites that have experienced hydrothermal interaction.

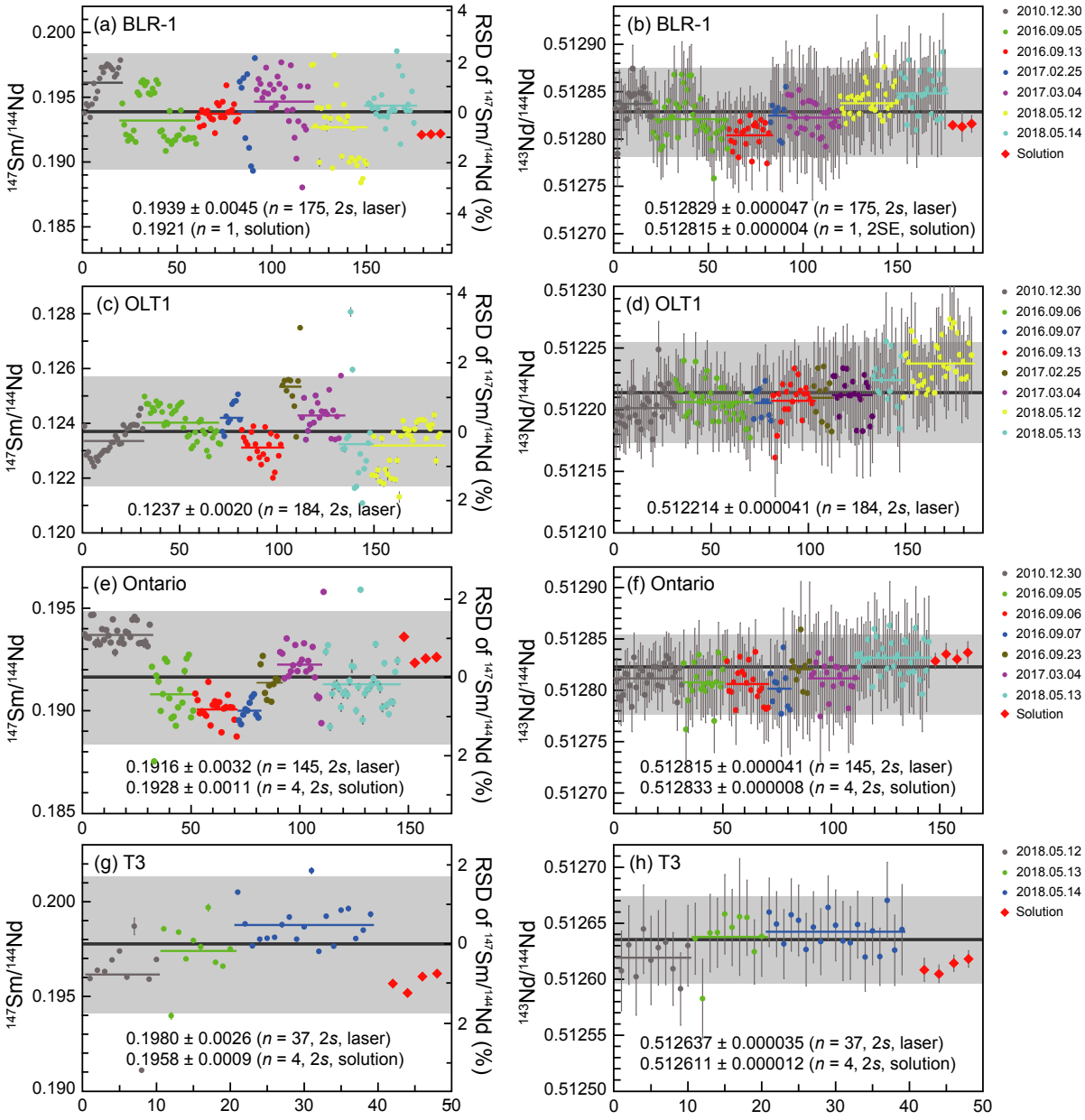

Figure 6. Measured $^{147}Sm/^{144}Nd$ and $^{143}Nd/^{144}Nd$ ratios of BLR-1 (a, b), OLT1 (c, d), Ontario (e, f) and T3 (g, h) titanites using LA-MC-ICP-MS. Error bars are 2SE (2 standard in-run errors); the mean values are shown as coloured lines for each data set; 2*s* uncertainties are shown as grey envelopes for long-term analyses using laser ablation. The red diamond with no rim represents data obtained by the solution method (ID-MC-ICP-MS) in the text. [Colour figure can be viewed at wileyonlinelibrary.com]

The U, Th and Pb mass fractions are 267 ± 25, 179 ± 19 and 55 ± 6 μg g^{-1}, respectively. It has a uniform Th/U ratio of 0.67 ± 0.03 and contains a relatively low proportion of f_{206} (%) (1.77 ± 0.31) and but high and scattered f_{208} (%) (22 ± 23) (Table 5). Most of the U-Pb data are clustered near the concordia, yielding consistent lower intercept and weighted mean $^{206}Pb/^{238}U$ ages of 1047 ± 6 Ma and 1047 ± 6 Ma (2*s*, *n* = 21), respectively (Figure 4d), within error.

$^{147}Sm/^{144}Nd$ values range from 0.1875 to 0.1959, with $^{143}Nd/^{144}Nd$ ranging from 0.512762 to 0.512863 (Figure 5d) from laser ablation analysis. The $^{147}Sm/^{144}Nd$ and $^{143}Nd/^{144}Nd$ values of 0.1928 ± 0.0011 and

0.512833 ± 0.000008 (*n* = 4, 2*s*), respectively, were determined by isotope dilution MC-ICP-MS with Sm and Nd mass fractions of 493 ± 23 and 1546 ± 71 μg g^{-1}, respectively (Table 4). Our long-term data set of *in situ* $^{143}Nd/^{144}Nd$ values for the Ontario titanite yields $^{147}Sm/^{144}Nd$ and $^{143}Nd/^{144}Nd$ mean values of 0.1916 ± 0.0032 and 0.512815 ± 0.000041 (*n* = 145, 2*s*), consistent with the reference value determined using solution methods (Figure 6e, f). The $^{145}Nd/^{144}Nd$ ratio has a mean value of 0.348424 ± 0.000039 (2*s*, *n* = 145), consistent with the recommended value. This titanite appears to be a very promising reference material for *in situ* Sm-Nd isotopic measurement.

MKED1

The MKED1 specimen used in this study was previously investigated by Spandler *et al.* (2016). It was derived from a euhedral crystal associated with calcite, extracted from a vein in skarn rocks in a diamond drill core recovered from *ca.* 80 m below the surface at the Elaine Dorothy prospect of the Mount Isa Inlier in Queensland, Australia. MKED1 is almost completely free of mineral inclusions and has a high degree of elemental and isotopic homogeneity (Figure 1e). It contains very low levels of common Pb and has homogeneous REE mass fractions characterised by significant LREE/HREE fractionation with a strong negative Eu anomaly. The MKED1 concordant $^{207}Pb/^{206}Pb$, $^{207}Pb/^{235}U$ and $^{206}Pb/^{238}U$ ages are 1521.02 ± 0.55 Ma, 1518.87 ± 0.31 Ma and 1517.32 ± 0.32 Ma (*n* = 5), respectively, using ID-TIMS methods. It is also remarkably uniform in $^{147}Sm/^{144}Nd$ and $^{143}Nd/^{144}Nd$ values. The TIMS measured $^{147}Sm/^{144}Nd$ ratio is 0.1270. The TIMS and LA-MC-ICP-MS $^{143}Nd/^{144}Nd$ data for MKED1 are 0.511630 ± 0.000003 (2*s*, *n* = 3) and 0.511645 ± 0.000037 (2*s*, *n* = 61), respectively, which are identical within error.

In our study, the chemical composition of the MKED1 chips was similar to that reported by Spandler *et al.* (2016) (Tables 1 and 3). The U, Th, Pb, Sm and Nd mass fractions measured by LA-ICP-MS are 106 ± 31, 321 ± 35, 49 ± 12, 336 ± 41 and 1559 ± 258 μg g^{-1}, respectively. Here, we used titanite YQ-82 as external reference material to calibrate MKED1, yielding a concordant age of 1517 ± 5 Ma (2*s*, *n* = 19, MSWD = 0.072; Figure 4e). *In situ* Sm-Nd isotope measurements yielded a $^{147}Sm/^{144}Nd$ ratio of 0.1286 ± 0.0027 (2*s*, *n* = 64) and a $^{143}Nd/^{144}Nd$ value of 0.511642 ± 0.000043 (2*s*, *n* = 64; Table 6, Figure 5e), which agree well with both the solution and laser ablation data in Spandler *et al.* (2016). The mean $^{145}Nd/^{144}Nd$ ratio of 0.348434 ± 0.000023 (2*s*, *n* = 64) obtained in this work is identical to the theoretical value of 0.348415 of Wasserburg *et al.* (1981), within error.

YQ-82

This titanite was collected from an alkaline dyke in Zhongtiao Mountain, Shanxi Province, China. It has very low to no initial common Pb compared with other titanites. The weighted mean $^{206}Pb/^{238}U$ age of the four grains is 1837.6 ± 1.0 Ma (MSWD = 1.3), measured by ID-TIMS (Huyskens et al. 2016).

A number of fragments from YQ-82 titanite were investigated with BSE and most of them were shown to contain abundant mineral inclusions, including quartz, biotite, calcite, plagioclase, K-feldspar and zircon (Figure 1f and Figure S1). The major and trace element compositions are reported in Tables 1 and 3. The Fe/Al a.p.f.u. ratio is *ca.* 0.46 and plots within the metamorphic field near the metamorphic–igneous dividing line. This titanite has relatively high and variable Y (2860 ± 2877 μg g^{-1}), and Nb (400 ± 307 μg g^{-1}) mass fractions. It is also heterogeneous in REE content and has a particularly variable HREE content with no obvious Eu anomaly (Eu/Eu* = 0.95 ± 0.50; Figure 2f). These variations could reflect the presence of mineral inclusions.

The U-Pb results for sixty-three analyses from this titanite are presented in Table 5. Mass fractions of U (60 ± 38 μg g^{-1}), Th (36 ± 25 μg g^{-1}) and Pb (22 ± 13 μg g^{-1}) show slight variations with a mean Th/U ratio of 0.67 ± 0.84 (2*s*, *n* = 63). It has a very low f_{206} (0.01 ± 0.32%) but relatively high and variable f_{208} (12 ± 20%). The data define a concordia line with an upper intercept age of 1841 ± 8 Ma (2*s*, *n* = 63; Figure 4f). A weighted mean $^{207}Pb/^{236}Pb$ age of 1840 ± 11 Ma (2*s*, *n* = 63) was obtained, which is in close agreement with the TIMS age of 1837.6 ± 1.0 Ma (Huyskens *et al.* 2016).

Titanite YQ-82 shows significant variability in $^{147}Sm/^{144}Nd$ and $^{143}Nd/^{144}Nd$ both inter- and intra-grain, but has a relatively uniform initial Nd isotopic composition. The $^{147}Sm/^{144}Nd$ values for YQ-82 titanite range from 0.1380 to 0.3306, with $^{143}Nd/^{144}Nd$ ranging from 0.511692 to 0.514043. All data scatter around a 1840 Ma reference isochron (Figure 5f). The $\varepsilon_{Nd}(t)$ based on an age of 1838 Ma is -3.86 ± 1.47 (2*s*, *n* = 28), and the mean $^{145}Nd/^{144}Nd$ of 0.348438 ± 0.000034 (2*s*, *n* = 28) is identical to the canonical value of 0.348415, within error.

T3

These coarse-grained titanite samples were collected from the Naresto Quarry, Arendal, southern Norway. The Arendal region is in the central part of Bamble lithotectonic domain, which is one of the classic transition zones from amphibolite-facies to granulite-facies regional metamorphism in a Proterozoic orogenic belt. Ages related to peak amphibolite- to granulite-facies metamorphism in the Arendal area range from 1140 to 1080 Ma, representing the first stage of the Sveconorwegian orogeny in response to continental collision (Nijland *et al.* 2014). Titanite from a carbonate vein near Arendal yielded a concordia age of 1103.5 ± 2.5 Ma (2*s*, *n* = 5), while an additional sample yielded an older titanite date (1137 ± 2 Ma; 2*s*, *n* = 1) using ID-TIMS (Cosca *et al.* 1998). Monazite from a garnet–sillimanite–quartz–biotite metapelite north of Arendal has a $^{207}Pb/^{235}U$ age of 1145 ± 3 Ma (2*s*, *n* = 1), which is interpreted as the approximate age of peak metamorphism (Cosca *et al.* 1998).

T3 titanite appears to be homogeneous in BSE images (Figure 1g), and LA-ICP-MS analyses indicate that it is very homogeneous in trace element abundances with particularly high REE mass fractions; Y (18648 ± 1069 μg g^{-1}) and Nb (2271 ± 351 μg g^{-1}) mass fractions are comparable to many other titanites. The chondrite-normalised REE plots show a 'seagull' pattern (La/Lu_N = 1.26 ± 0.04) with a negative Eu anomaly (Eu/Eu* = 0.19 ± 0.00; Figure 2g).

The U-Pb results for twenty-one fragments are presented in Table 5 and on a TW concordia diagram in Figure 3g. The U (296 ± 17 μg g^{-1}), Th (281 ± 13 μg g^{-1}) and Pb (63 ± 3 μg g^{-1}) mass fractions are relatively homogeneous with a Th/U ratio of 0.95 ± 0.07. It has very low levels of common Pb (f_{206} = -0.02 ± 0.28%). The data define a concordia age of 1138 ± 6 Ma (2*s*, *n* = 21). A weighted mean $^{207}Pb/^{206}Pb$ age of 1125 ± 14 Ma (2*s*, *n* = 21) was obtained (Figure 4g).

Solution MC-ICP-MS analysis of four separate chips of T3 gave very similar Sm-Nd isotopic compositions (Table 4). Measured $^{147}Sm/^{144}Nd$ and $^{143}Nd/^{144}Nd$ ratios are *ca.* 0.1958 and 0.512611, respectively, which gives a mean $\varepsilon_{Nd}(t)$ value of -0.39 ± 0.11 (2*s*) with Sm and Nd mass fractions of 1884 ± 106 and 5817 ± 331 μg g^{-1}, respectively (Table 4). To test isotopic homogeneity at the sub-mm scale, we undertook thirty-seven *in situ* measurements by LA-MC-ICP-MS on thirty separate chips of T3. Results are presented in Figures 5g and 6g, h. The *in situ* laser ablation data gave slightly higher $^{147}Sm/^{144}Nd$ and $^{143}Nd/^{144}Nd$ ratios of 0.1980 ± 0.0026 (2*s*, *n* = 37) and 0.512637 ± 0.000035 (2*s*, *n* = 37), respectively, yielding a mean $\varepsilon_{Nd}(t)$ value of -0.20 ± 0.61 (2*s*, *n* = 37), which agrees with the values obtained by isotope dilution methods within uncertainty. Overall, no significant isotopic variation is observed between or within chips.

T4

T4 was collected from the Sjaen Quarry, Kragerø, southern Norway. Grains of the material are 2–3 mm in diameter, dark brown to black in colour and unzoned in BSE images (Figure 1h). The Kragerø area is located in the north of Bamble Sector. Zircon, monazite and titanite U-Pb ages in coastal samples from the Bamble domain place the beginning of high-grade metamorphism at around 1140 Ma (Cosca *et al.* 1998, Engvik *et al.* 2016). Titanites from a pegmatite and a calc-silicate near Kragerø have ages of 1104–1107 Ma (Cosca *et al.* 1998). Dolomite marbles in the Kragerø area have age-corrected ε_{Nd} values ranging from +0.7 to -1.5 (Dahlgren *et al.* 1992).

Trace element compositions are reported in Table 3. T4 has abundant and variable Y (866 ± 1007 μg g^{-1}) but relatively low Zr (183 ± 121 μg g^{-1}) and Nb (289 ± 181 μg g^{-1}) mass fractions compared with other titanites. The total REE mass fractions show some variation and yield consistent chondrite-normalised REE patterns with highly fractionated LREE, relatively flat HREE patterns (Figure 2h) and slightly positive Eu anomalies (1.15 ± 0.39).

The U, Th and Pb mass fractions are 110 ± 127, 62 ± 61 and 23 ± 25 μg g^{-1}, respectively. The measured f_{206} values are generally low and vary from -0.2 to 0.9% (mean = 0.25 ± 0.54%), reflecting a minor component of common Pb in the T4 titanite (Table 5 and Table S3). U-Pb data obtained by LA-ICP-MS returned a lower intercept age of 1132 ± 7 Ma (2*s*, *n* = 20). After ^{207}Pb correction, the data yielded a weighted mean $^{206}Pb/^{238}U$ age of 1131 ± 8 Ma (2*s*, *n* = 20; Figure 4h).

The $^{147}Sm/^{144}Nd$ ratios of T4 titanite are quite variable (0.0785–0.1496) and accompanied by a ~ 550 ppm increase in $^{143}Nd/^{144}Nd$. The $^{147}Sm/^{144}Nd$ and $^{143}Nd/^{144}Nd$ values positively correlate (Figure 5h) and scatter around the reference line (1130 Ma). This variation was observed within a single grain and between grains. A mean initial $^{143}Nd/^{144}Nd$ value of 0.511174 ± 0.000060 (2*s*, *n* = 75) was calculated at the reference age of 1130 Ma (Table 6). One fragment was studied using ID-MC-ICP-MS, and yielded $^{147}Sm/^{144}Nd$ of 0.0924 and initial $^{143}Nd/^{144}Nd$ ratio of 0.511161 ± 0.000008 (2*s*). The calculated $\varepsilon_{Nd}(t)$ value based on an age of 1130 Ma is -0.36.

Table 7.
Compilation of Sm and Nd mass fractions and Sm-Nd isotopic data of titanite in this study

Titanite	Sm (μg g^{-1}) (± 2*s*)	Nd (μg g^{-1}) (± 2*s*)	[^{147}Sm/^{144}Nd]$_m$ (± 2*s*)	2 RSD (%)	[^{143}Nd/^{144}Nd]$_m$ (± 2*s*)	(^{143}Nd/^{144}Nd)$_t$ (± 2*s*)	$\varepsilon_{Nd}(t)$ (± 2*s*)	Method	References
Khan (~ 518 Ma)									
			0.1188 (50)	4.2	0.511642 (41)	0.511238 (39)	-14.3 (0.8)	LA-MC-ICP-MS	This study
					0.511635 (28)			LA-MC-ICP-MS	Xu *et al.* (2015b)
			0.1217 (02)	0.2	0.511632 (30)	0.511219 (29)	-14.7 (0.6)	LA-MC-ICP-MS	Xu *et al.* (2018)
			0.1218 (02)	0.2	0.511648 (19)	0.511235 (18)	-14.4 (0.4)	LA(fs)-MC-ICP-MS	Xu *et al.* (2018)
BLR-1 (~ 1047 Ma)									
	439	1381	0.1921		0.512815 (04)	0.511495	4.07	Sol.-MC-ICP-MS	This study
			0.1939 (45)	2.3	0.512829 (47)	0.511496 (49)	4.10 (0.96)	LA-MC-ICP-MS	This study
			0.1982 (48)	2.4	0.512818 (82)	0.511456 (49)	3.32 (1.73)	LA-MC-ICP-MS	Xu *et al.* (2018)
			0.1966 (54)	2.7	0.512812 (110)	0.511461 (73)	4.42 (2.27)	LA(fs)-MC-ICP-MS	Xu *et al.* (2018)
OLT1 (~ 1015 Ma)									
			0.1237 (20)	1.6	0.512214 (41)	0.511390 (44)	1.20 (0.86)	LA-MC-ICP-MS	This study
					0.512270 (24)			LA-MC-ICP-MS	Xu *et al.* (2015b)
			0.1313 (19)	1.4	0.512270 (26)	0.511396 (13)	1.32 (0.57)	LA-MC-ICP-MS	Xu *et al.* (2018)
			0.1307 (24)	1.8	0.512272 (32)	0.511402 (16)	1.44 (0.70)	LA(fs)-MC-ICP-MS	Xu *et al.* (2018)
Ontario (~ 1053 Ma)									
	493 (23)	1546 (71)	0.1928 (11)	0.5	0.512833 (08)	0.511501 (14)	4.34 (0.28)	Sol.-MC-ICP-MS	This study
			0.1916 (32)	1.7	0.512815 (41)	0.511490 (40)	4.15 (0.79)	LA-MC-ICP-MS	This study
MKED1 (~ 1521 Ma)									
	345 (34)	1641 (158)	0.1270 (08)	0.6	0.511630 (07)	0.510360	-6.09 (0.21)	TIMS	Spandler *et al.* (2016)
			0.1286 (27)	2.1	0.511642 (43)	0.510356 (45)	-6.17 (0.89)	LA-MC-ICP-MS	This study
YQ-82 (~ 1838 Ma)									
			0.2556 (921)	36	0.513154 (1106)	0.510063 (75)	-3.86 (1.47)	LA-MC-ICP-MS	This study
T3 (~ 1130 Ma)									
	1884 (106)	5817 (331)	0.1958 (09)	0.5	0.512611 (12)	0.511159 (06)	-0.39 (0.11)	Sol.-MC-ICP-MS	
			0.1980 (26)	1.3	0.512637 (35)	0.511169 (31)	-0.20 (0.61)	LA-MC-ICP-MS	This study
T4 (~ 1130 Ma)									
	96	628	0.0924		0.511846 (08)	0.511161	-0.36	Sol.-MC-ICP-MS	This study
			0.0979 (333)	34	0.511901 (239)	0.511174 (60)	-0.09 (1.18)	LA-MC-ICP-MS	This study
TLS-36 (~ 135 Ma)									
	506 (31)	2973 (142)	0.1033 (01)	2.8	0.512270 (10)	0.512179 (11)	-5.56 (0.21)	Sol.-MC-ICP-MS	This study
			0.1032 (124)	12	0.512265 (60)	0.512174 (60)	-5.66 (1.17)	LA-MC-ICP-MS	This study
NW-IOA (~ 130 Ma)									
	316	1738	0.1029 (29)		0.512143 (09)	0.512049	-8.22	Sol.-MC-ICP-MS	This study
			0.1090 (88)	8.1	0.512147 (56)	0.512054 (54)	-8.12 (1.05)	LA-MC-ICP-MS	This study
Pakistan (~ 21 Ma)									
	170 (49)	579 (160)	0.1774 (25)	1.4	0.512149 (25)	0.512126 (25)	-9.49 (0.48)	Sol.-MC-ICP-MS	This study
			0.1756 (107)	6.1	0.512137 (69)	0.512114 (68)	-9.72 (1.33)	LA-MC-ICP-MS	This study
C253 (~ 20 Ma)									
	203 (17)	670 (64)	0.1835 (18)	1.0	0.512138 (11)	0.512114 (12)	-9.72 (0.23)	Sol.-MC-ICP-MS	This study
			0.1857 (113)	6.1	0.512146 (70)	0.512122 (70)	-9.56 (1.36)	LA-MC-ICP-MS	This study

TLS-36

TLS-36 titanite used in this study was previously studied by Li *et al.* (2010) and derived from the Tonglushan Cu-Fe-Au skarn ore-related Yangxin quartz diorite intrusion. Previous SIMS zircon U-Pb dating indicated that the Yangxin quartz diorite was emplaced at 138.5 ± 2.5 Ma (2*s*, *n* = 14) and titanite from the same host rocks yielded a weighted mean ^{206}Pb/^{238}U age of 136.0 ± 1.5 Ma (2*s*, *n* = 12) using LA-ICP-MS (Li *et al.* 2010).

A number of fragments from this titanite were examined with BSE and display some fractures (Figure 1i). Some contain abundant mineral inclusions consisting of hornblende, K-feldspar, apatite and quartz. The major and trace element compositions are reported in Tables 1 and 3. The Fe/Al a.p.f.u. ratio is 0.84 and plots in the igneous field. TLS-36 titanite contains high Y (1441 ± 538 μg g^{-1}), Zr (339 ± 123 μg g^{-1}) and Nb (1612 ± 678 μg g^{-1}). The REE mass fractions are relatively heterogeneous and the chondrite-normalised REE pattern is highly fractionated

(mean La/Lu_N = 21.5 ± 5.5) with no obvious Eu anomaly (Eu/Eu* = 0.91 ± 0.10; Figure 2i).

The U-Pb results are presented in Table 5 and on a TW concordia diagram in Figure 4i. The U (51 ± 18 μg g^{-1}), Th (418 ± 231 μg g^{-1}) and Pb (4.2 ± 1.7 μg g^{-1}) mass fractions are relatively uniform with a Th/U ratio of 8.08 ± 2.1 (2*s*). The common Pb mass fractions (f_{206}) are high, ranging from 13.3 to 26.8% with a mean value of 17.6 ± 6.8% (2*s*), which is similar to f_{208} with a mean value of 13.8 ± 5.8% (2*s*, *n* = 23; Table 5 and Table S3). All data are clustered near the concordia, yielding a lower intercept age of 136 ± 2 Ma (2*s*, *n* = 23), consistent with the ^{207}Pb-corrected weighted mean $^{206}Pb/^{238}U$ age of 135 ± 2 Ma (2*s*, *n* = 23).

The Sm (506 ± 31 μg g^{-1}) and Nd (2973 ± 142 μg g^{-1}) mass fractions are relatively high compared with other titanites (Table 4). The $^{147}Sm/^{144}Nd$ values range from 0.0833 to 0.1192, with $^{143}Nd/^{144}Nd$ values ranging from 0.512199 to 0.512353. The data scatter around the reference line of 135 Ma (Figure 5i), and the calculated $\varepsilon_{Nd}(t)$ based on an age of 135 Ma is -5.66 ± 1.17 (2*s*, *n* = 80), which agrees well with the ID-MC-ICP-MS result of -5.56 ± 0.21 (Table 7). The mean $^{145}Nd/^{144}Nd$ is 0.348434 ± 0.000030 (2*s*, *n* = 80), consistent with the reference value within error (Table 6).

NW-IOA

This titanite, previously studied by Liu *et al.* (2018), was collected from diopside–anhydrite-altered rocks in the hanging wall of the deep ore body (*ca.* 1500–1600 m depth) in the Luohe Fe deposit, the largest magnetite–apatite (MA)-type deposit in the Middle-Lower Yangtze River Valley Metallogenic Belt (MLYB), located in the western Lu-Zong volcanic basin in eastern China. The titanite is relatively fresh and occurs in clusters with magnetite (locally as euhedral inclusions), diopside, epidote, apatite and anhydrite. Widespread titanite mineralisation is developed in both the footwall of shallow ore bodies and the hanging wall of deep ore bodies. Recent LA-ICP-MS titanite U-Pb dating results reported by Liu *et al.* (2018) yielded a U-Pb intercept age of 129.5 ± 0.5 Ma and a ^{207}Pb-corrected $^{206}Pb/^{238}U$ weighted mean age of 129.7 ± 0.8 Ma (2*s*, *n* = 21, MSWD = 1.3).

BSE imaging shows that NW-IOA is not homogeneous, and minor anhydrite was noted (Figure 1j). This titanite has abundant Y (736 ± 406 μg g^{-1}) and Zr (351 ± 593; Table 3). It has a small range of REE mass fractions, and the chondrite-normalised REE pattern is highly fractionated (mean La/Lu_N = 15.7 ± 20.5) with no obvious Eu anomaly (Eu/Eu* = 0.88 ± 0.53; Figure 2j).

The U-Pb results from this work are presented in Table 5 and Figure 4j. NW-IOA contains equivalent U (254 ± 198 μg g^{-1}) and Th (221 ± 333 μg g^{-1}) mass fractions, and a Pb mass fraction of 6.6 ± 4.6 μg g^{-1}. The measured f_{206} was found to vary from 0.4 to 3.8%. Twenty analyses were plotted on a TW diagram and yielded a lower intercept age of 130 ± 1 Ma (2*s*, MSWD = 1.6) and a ^{207}Pb-corrected weighted mean $^{206}Pb/^{238}U$ age of 130 ± 1 Ma (2*s*, MSWD = 1.5), in good agreement with previous studies (Liu *et al.* 2018).

Solution MC-ICP-MS analysis yielded $^{147}Sm/^{144}Nd$ of 0.1100 and $^{143}Nd/^{144}Nd$ of 0.512143 ± 0.000009 (2*s*) with Sm and Nd mass fractions of 316 and 1738 μg g^{-1}, respectively (Table 4). The $^{147}Sm/^{144}Nd$ values determined by laser ablation on NW-IOA range from 0.1020 to 0.1268, with $^{143}Nd/^{144}Nd$ ranging from 0.512104 to 0.512224 (Figure 5j). All data give a mean $\varepsilon_{Nd}(t)$ value of -8.12 ± 1.05 (2*s*, *n* = 80), within uncertainty of the -8.22 calculated from the solution analysis (Tables 4, 6 and 7). The mean $^{145}Nd/^{144}Nd$ ratio of 0.348433 ± 0.000034 (2*s*, *n* = 80) is in close agreement with the reference value.

Pakistan

This euhedral, light green gem-quality titanite (2.5 cm × 1.5 cm × 1 cm) was obtained from a gem collector. It is typically homogeneous in BSE images (Figure 1k). Mean major and trace element compositions (Tables S1 and S3) show that this titanite has an extremely low Fe/Al a.p.f.u ratio of 0.09 and that it is enriched in Y (645 ± 189 μg g^{-1}) and Nb (2110 ± 1099 μg g^{-1}). It has a slightly heterogeneous REE distribution, and REE contents increase from La to Nd. The chondrite-normalised REE pattern shows minor fractionation (mean La/Lu_N = 1.39 ± 0.50) with an obvious Eu anomaly (Eu/Eu* = 0.62 ± 0.04; Figure 2k). The Sm and Nd mass fractions are 170 ± 49 and 579 ± 160 μg g^{-1}, respectively, obtained by the solution method (Table 4).

The U-Pb results can be found in Table 5. The measured U, Th and Pb mass fractions are 86 ± 29, 257 ± 59 and 0.49 ± 0.16 μg g^{-1}, respectively. The mean Th/U ratio is 3.07 ± 1.1. The measured f_{206} values are generally low and vary between -1.2 and 3.8% with a mean of 1.1 ± 2.7% (2*s*, *n* = 22). Twenty-two spot analyses were plotted on the TW diagram and yielded a lower intercept age of 21.5 ± 0.4 Ma (2*s*). After ^{207}Pb correction, a

weighted mean $^{206}Pb/^{238}U$ age of 21.4 ± 0.4 Ma (2*s*, MSWD = 2.1) was calculated (Figure 4k).

The Pakistan titanite has variations in $^{147}Sm/^{144}Nd$ and $^{143}Nd/^{144}Nd$, but has a uniform initial Nd isotopic composition. The *in situ* measurements yielded $^{147}Sm/^{144}Nd$ ranging from 0.1640 to 0.1921 and $^{143}Nd/^{144}Nd$ from 0.512028 to 0.512207 (Figure 5k). A calculated mean $\varepsilon_{Nd}(t)$ of -9.72 ± 1.33 based on an age of 20 Ma was determined, which agrees with result obtained using solution methods (-9.49 ± 0.48; Tables 4, 6 and 7). The $^{145}Nd/^{144}Nd$ ratios determined by laser ablation and solution are identical within error and give a mean value of 0.348429 ± 0.000036 (2*s*, *n* = 80).

C253

This titanite is a large, light yellow-green crystal (1.5 × 1 × 0.5 cm) from Xinjiang, China, provided by a gem collector. It is typically homogeneous in BSE images (Figure 1l). Major element compositions are listed in Table 1, yielding a Fe/Al a.p.f.u. ratio of 0.41 and a composition that plots in the metamorphic field. Trace element mass fractions presented in Table 3 demonstrate that this titanite has abundant Y (768 ± 70 μg g^{-1}) and Nb (533 ± 50 μg g^{-1}). As shown in the chondrite-normalised REE patterns, C253 is homogeneous in REE distribution, with contents increasing from La to Sm. It shows a slight LREE/HREE fractionation (1.37 ± 0.6) with a negative Eu anomaly (0.71 ± 0.02), showing a 'seagull' pattern on chondrite-normalised plots, with more enrichment in LREE (Figure 2l).

The U (39 ± 2 μg g^{-1}), Th (214 ± 10 μg g^{-1}) and Pb (0.31 ± 0.09 μg g^{-1}) mass fractions and Th/U ratio (5.45 ± 0.44) obtained from these fractions are relatively uniform. Common Pb mass fraction in most analyses is low, and f_{206} is between -3.8 and 11.8% with a mean of 8.04 ± 5.86% (Table 5 and Table S3). Twenty analyses yielded a lower intercept age of 19.6 ± 0.3 Ma (2*s*) on a TW diagram. The ^{207}Pb-corrected weighted mean $^{206}Pb/^{238}U$ age is 19.5 ± 0.4 Ma (2*s*, *n* = 20, MSWD = 1.5) after ^{207}Pb correction (Figure 4l).

The Sm (203 ± 17 μg g^{-1}) and Nd (670 ± 64 μg g^{-1}) mass fractions of C253 presented in Table 4 are lower than those in other frequently used reference materials such as Khan, BLR-1 and OLT1, creating a larger error in measured $^{143}Nd/^{144}Nd$ ratios. Thus, this C253 titanite might not be suitable as reference material for *in situ* Nd isotope measurement. The $^{147}Sm/^{144}Nd$ ratios are relatively uniform, ranging from 0.1757 to 0.1949, whereas the $^{143}Nd/^{144}Nd$ ratios are slightly scattered, ranging from 0.512059 to 0.512264 with a mean of 0.512146 ± 0.000070 (2*s*, *n* = 64; Figure 5l). The $\varepsilon_{Nd}(t)$ of -9.56 ± 1.36 (2*s*, *n* = 64), calculated based on an age of 20 Ma, agrees with the reference value obtained using solution methods (Tables 4, 6 and 7). The measured $^{145}Nd/^{144}Nd$ gave a mean value of 0.348434 ± 0.000054 (2*s*, *n* = 64), which is identical to the recommended value of 0.348415 (Wasserburg *et al.* 1981).

Discussion

Common Pb incorporation into titanite

At the time of writing, the mechanism of common Pb incorporation into different types of titanite crystals has not been extensively explored (Olierook *et al.* 2018). In contrast to zircon, titanite frequently accommodates significant amounts of common Pb in its crystal lattice. Much of the common Pb in titanite is trapped during mineral growth, and thus, the composition of common Pb can vary significantly depending on the local crystallisation environment (Kirkland *et al.* 2016, 2018).

As shown in Figure 7, a large range of common Pb mass fractions is observed in magmatic and hydrothermal samples, whereas common Pb in high-grade metamorphic titanites is relatively low and uniform. Most magmatic titanites have initial U mass fractions of 10–1000 μg g^{-1}. Plots of total U mass fraction versus f_{206} (%) reveal a broadly negative correlation, where greater U is typically associated with a lower common Pb component. For example, there is a strong negative correlation between U mass fraction and f_{206} (%) for titanites from potassic alkaline igneous rocks in the Sanjiang area (south-western China; LC1605 and BSZ1604) and a similar pattern is observed in titanite TLS-36 and Qinghu (Figure 7a). However, YQ-82 deviates from this pattern with very low common Pb mass fractions. High-temperature metamorphic titanites in skarn and granulite-facies metamorphic rocks have moderate-to-high (~ 100 to ~ 400 μg g^{-1}) and uniform U mass fractions, combined with a low f_{206} (%) (zero to < 3%) (e.g., BLR-1, OLT1, Ontario, MKED1, T3 and T4; Figure 7b). Titanites in pegmatite and hydrothermal mineral deposits have more variable common Pb mass fractions. For instance, Khan has high U (~ 1000 μg g^{-1}) and low common Pb (< 4%), and L76 has low U (~ 20 μg g^{-1}) and high common Pb (~ 100%; Figure 7c and Table 5s). There is no association between f_{206} (%) and total REE content. Since U and REE substitute for Ca^{2+} in a sevenfold-co-ordinated site, incorporation of these ions might happen at the same time. The implication is that a negative correlation between U mass fraction and f_{206} (%) results from the radioactive production of Pb from U, rather than a differential uptake of Pb during mineral crystallisation.

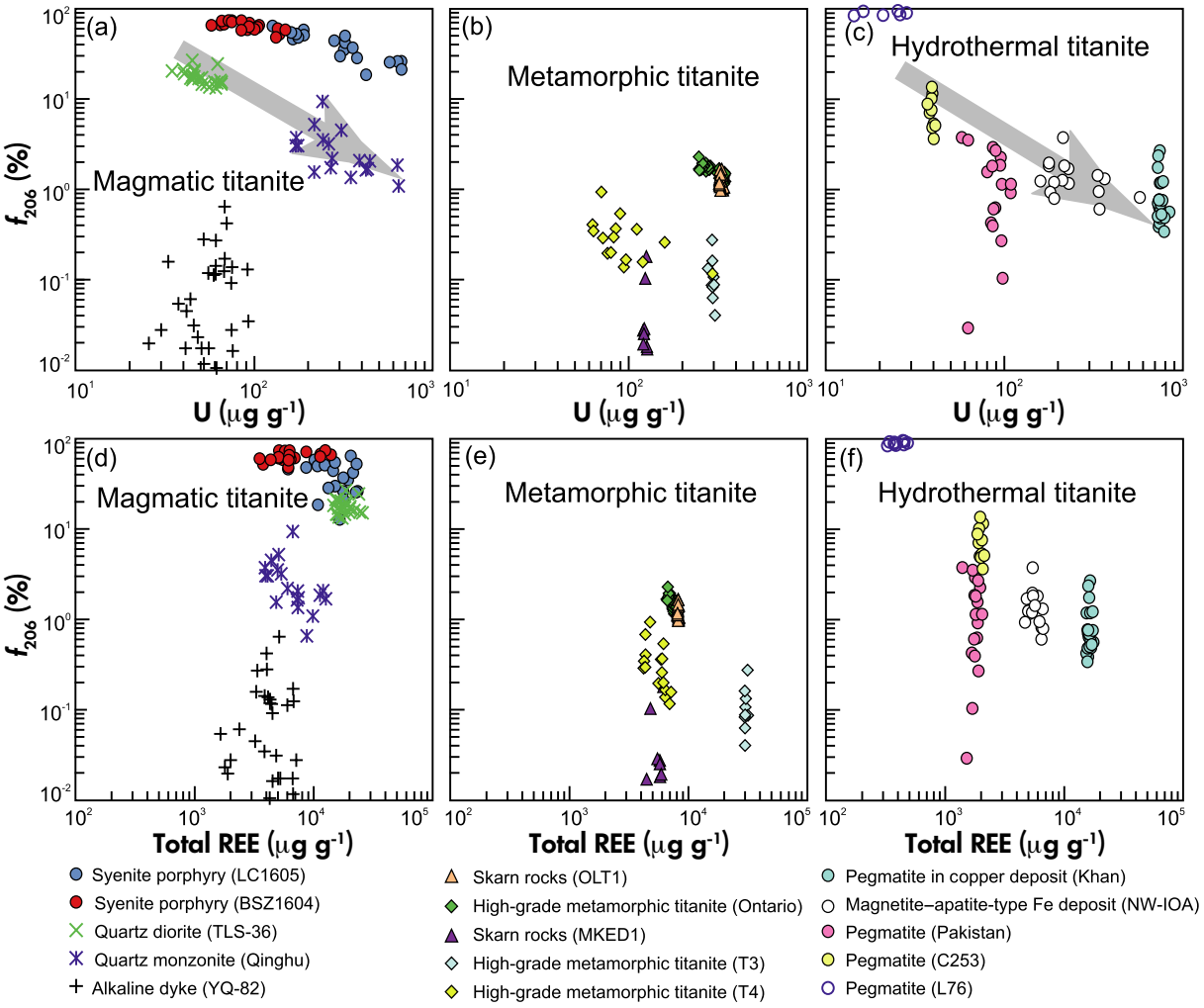

Figure 7. The variation between U (μg g^{-1}) versus f_{206} (%) (a–c) and total REE versus f_{206} (%) (d–f) in different titanites. Data are attached in Table S5. [Colour figure can be viewed at wileyonlinelibrary.com]

Evaluation of potential *in situ* U-Pb titanite reference materials

The U-Pb ages of the titanites examined in this study are summarised in Table 5. It has been demonstrated that MKED1 is an excellent reference material for U-Pb dating (Spandler *et al.* 2016), and therefore, it was used as a calibrator in this study. Although Khan is a good reference material for U-Pb dating, its $^{207}Pb/^{206}Pb$ ratio shows slight variation (Kinny *et al.* 1994, Heaman 2009). The U-Pb system in BLR-1, OLT1 and Ontario is chemically and isotopically uniform with weighted mean $^{206}Pb/^{238}U$ ages calculated after ^{207}Pb correction being consistent with previously reported ID-TIMS ages. This confirms the robustness of these titanites as U-Pb geochronological reference materials (Aleinikoff *et al.* 2007, Kennedy *et al.* 2010, Sun *et al.* 2012, Spencer *et al.* 2013, Horstwood *et al.* 2016). YQ-82 titanite is relatively concordant, although some analyses are somewhat reversely discordant, which might result from the loss of U or migration of Pb. T3 and T4 are largely free of inclusions and homogeneous at the level of measurement precision required for U-Pb dating. NW-IOA titanite also displays some variation in $^{207}Pb/^{206}Pb$ ratios given numerous mineral inclusions, and this precludes it from being a suitable U-Pb dating reference material even though it contains little common Pb. TLS-36 titanite has relatively higher and variable common Pb, but the ^{207}Pb-corrected weighted mean $^{206}Pb/^{238}U$ age obtained in this work (135 ± 2 Ma) is in agreement with previously published LA-ICP-MS data within error (Li *et al.* 2010). C253 has relatively scattered $^{207}Pb/^{206}Pb$ ratios, indicting it is an unsuitable U-Pb dating reference material. Pakistan is almost concordant with an age of 21 Ma and can be used as a reference material for determining U-Pb ages of

Cenozoic titanite samples, but it has a relatively low U mass fraction and is too young to be a suitable primary age reference material for the majority of titanite unknowns.

In summary, BLR-1, OLT1, Ontario, MKED1 and T3 titanites are excellent reference materials for U-Pb dating. Pakistan titanite can be employed as a reference material for *in situ* dating young titanite samples. YQ-82 titanite could be a good potential reference material for *in situ* U-Pb analysis because it has no common Pb; however, the internal structures and mineral inclusions in this titanite will require careful selection of suitable target domains.

Matrix-matched strategy for *in situ* Sm-Nd analysis of titanite

Precise and accurate $^{147}Sm/^{144}Nd$ measurements are critical for robust initial $^{143}Nd/^{144}Nd$ ratios and $\varepsilon_{Nd}(t)$ values, especially for ancient geological samples. The potential ε_{Nd} deviation from true values with time for 0–10% of $^{147}Sm/^{144}Nd$ uncertainty, with a $^{147}Sm/^{144}Nd$ of 0.2, is shown in Figure 8. For a ~ 1000 Ma titanite, in order to achieve initial $^{143}Nd/^{144}Nd$ with an uncertainty of < 0.5ε, $^{147}Sm/^{144}Nd$ must be measured with analytical error at the < 2% level. Therefore, the principal technical limitation is the accuracy of $^{147}Sm/^{144}Nd$ measurements.

The impact of non-matrix matching on $^{147}Sm/^{144}Nd$ fractionation during laser ablation is still controversial. Liu *et al.* (2012) observed a significant difference (*ca.* 7%) in the $^{147}Sm/^{144}Nd$ ratios of apatite and monazite, whereas no $^{147}Sm/^{144}Nd$ fractionation was observed between monazite and LREE glass. We have measured β_{Sm} and β_{Nd} for titanite reference materials over a 2 years period. The β_{Sm} and β_{Nd} values were directly obtained from the titanite samples themselves during *in situ* analysis and calculated by normalising $^{147}Sm/^{149}Sm$ and $^{146}Nd/^{144}Nd$ ratios to 1.08680 (Dubois *et al.* 1992) and 0.7219 (O'Nions *et al.* 1977) by the exponential law (Equations 1 and 2).

$$\beta_{Sm} = \frac{\ln\left(\frac{\left[^{147}Sm/^{149}Sm\right]_{ref}}{\left[^{147}Sm/^{149}Sm\right]_{meas}}\right)}{\ln\left(\frac{M^{147}_{Sm}}{M^{149}_{Sm}}\right)} \quad (1)$$

$$\beta_{Nd} = \frac{\ln\left(\frac{\left[^{146}Nd/^{144}Nd\right]_{ref}}{\left[^{146}Nd/^{144}Nd\right]_{meas}}\right)}{\ln\left(\frac{M^{146}_{Nd}}{M^{144}_{Nd}}\right)} \quad (2)$$

The correlation between β_{Sm} and β_{Nd} for all measured titanites is presented in Figure 9. All analyses show highly correlated β_{Sm}–β_{Nd} with a linear regression line of $\beta_{Nd} = 0.997*\beta_{Sm} - 0.1986$ ($R^2 = 0.9964$). Other researchers have monitored β_{Sm} and β_{Nd} for different reference materials, including apatite, titanite, allanite, monazite and LREE glass, and obtained a β_{Sm}–β_{Nd} correlation similar to the results in this work, indicating a long-term stability of our method (Fisher *et al.* 2011, Liu *et al.* 2012, Yang *et al.* 2013, Xu *et al.* 2018). In this work, a matrix-matched natural titanite reference material was used during laser ablation to calibrate elemental fractionation and instrumental drift, thereby minimising issues associated with laser-induced fractionation on $^{147}Sm/^{144}Nd$ (Yang *et al.* 2014). As shown in Table 7, the $^{147}Sm/^{144}Nd$ and $^{143}Nd/^{144}Nd$ values for MKED1 obtained by laser ablation are consistent with the results measured by solution methods, verifying the reliability of this approach.

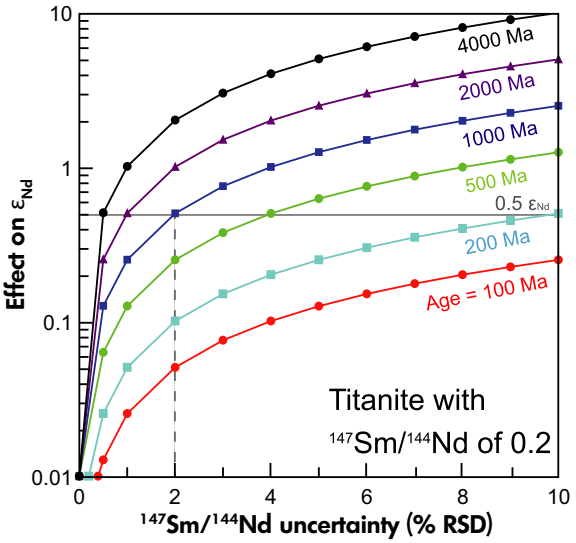

Figure 8. Effects on $\varepsilon_{Nd}(0)$ of radiogenic in-growth ^{143}Nd in titanites with variable crystallisation age and a $^{147}Sm/^{144}Nd$ ratio of 0.2. For samples older than 1000 Ma, to achieve precision of 0.5ε for the determination of initial $^{143}Nd/^{144}Nd$, the measurement of $^{147}Sm/^{144}Nd$ is required to a precision of < 2%. [Colour figure can be viewed at wileyonlinelibrary.com]

Potential titanite reference materials for *in situ* Sm-Nd isotopic analysis

Ideal reference materials for *in situ* Sm-Nd isotopic measurement by LA-MC-ICP-MS should meet the following requirements: (a) display isotopic homogeneity in $^{147}Sm/^{144}Nd$ and $^{143}Nd/^{144}Nd$ ratios on the scale of the laser spot employed; (b) possess uniform distributions of Sm

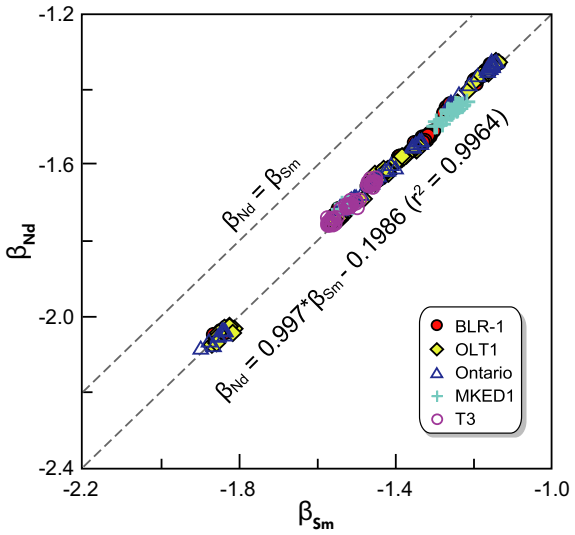

Figure 9. Correlation between β_{Sm} and β_{Nd} of BLR-1, OLT1, Ontario, MKED1 and T3 done in our laboratory. [Colour figure can be viewed at wileyonlinelibrary.com]

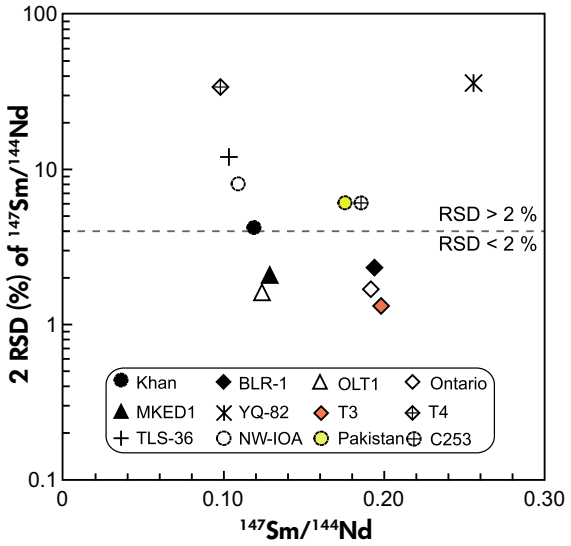

Figure 10. Variation in $^{147}Sm/^{144}Nd$ ratios for titanites investigated in this study. 2 RSD (%) (relative standard deviation) is used to evaluate the degree of variation. The values are listed in Table 6. [Colour figure can be viewed at wileyonlinelibrary.com]

and Nd, and a sufficiently high Nd mass fraction to allow Nd to be measured precisely; (c) lack internal structures (e.g., cracks) and mineral inclusions; (d) possess a known crystallisation age to facilitate calculation of the initial Nd isotopic signature; and (e) be sufficiently abundant so that material can be distributed to the scientific community (Yang *et al.* 2009, 2014, Liu *et al.* 2012, Spandler *et al.* 2016, Xu *et al.* 2018).

Based on the *in situ* measurement of the Sm-Nd isotopic composition of twelve natural titanites, most have significant variations in $^{147}Sm/^{144}Nd$ ratios with RSD > 2% (Figure 10), indicating they are not suitable as Sm-Nd isotope reference materials. BLR-1, OLT1, MKED1, Ontario and T3 are potential titanite reference materials since they have abundant Nd and are relatively homogeneous in $^{147}Sm/^{144}Nd$ with a relative standard deviation of less than 2% according to our data. As shown in Figure 6, long-term *in situ* measurement of $^{147}Sm/^{144}Nd$ and $^{143}Nd/^{144}Nd$ in BLR-1, OLT1, Ontario and T3 is reproducible. The LA-MC-ICP-MS *in situ* analyses of titanites investigated in this study agree within uncertainty with values obtained by the solution method (Figure 11).

Due to limited supply during this study, OLT1 was not analysed by the solution method; however, based on the robustness of our *in situ* Sm-Nd analyses, the Sm-Nd isotopic composition of OLT1 is reproducible and accurate. The ID-MC-ICP-MS result is the preferred reference value for BLR-1, Ontario and T3 titanites.

The results of this work suggest that BLR-1, OLT1, Ontario and T3 can be used as reference materials, and we evaluate MKED1 as a good reference material for *in situ* Sm-Nd isotopic measurement. The studied titanites Ontario, T3 and Pakistan were also homogeneous in Pb isotopic

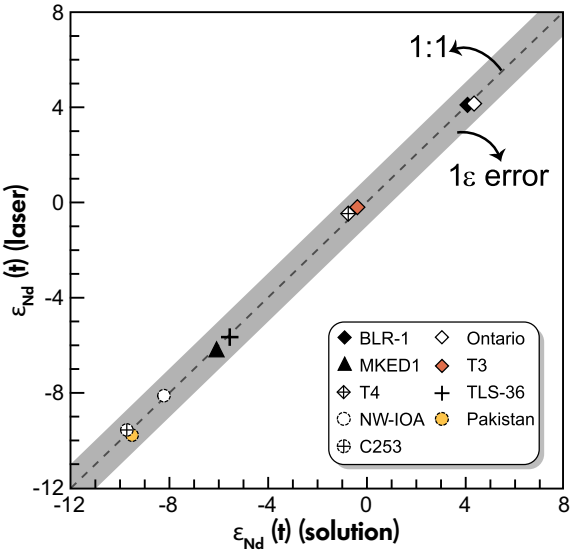

Figure 11. Plots of $\varepsilon_{Nd}(t)$ (solution) versus $\varepsilon_{Nd}(t)$ (laser) of titanites investigated in this study. [Colour figure can be viewed at wileyonlinelibrary.com]

composition, which, together with their large crystal size (and hence abundance of material), makes them excellent candidates for use as reference materials for *in situ* U-Pb dating, although TIMS analyses are needed to determine their precise ages. We are willing to distribute Ontario, T3 and Pakistan reference materials upon request to other laboratories.

Conclusions

Considering the increasing demand for titanite reference materials for *in situ* U-Pb and/or Sm-Nd isotopic analysis, this work investigated *in situ* U-Pb ages and Sm-Nd isotope measurement results of four well-known titanite reference materials (Khan, BLR-1, OLT1 and MKED1) and eight potential candidate reference materials (Ontario, YQ-82, T3, T4, TLS-36, NW-IOA, Pakistan and C253) using LA-(MC)-ICP-MS and ID-MC-ICP-MS. For U-Pb dating, using MKED1 titanites as a calibration reference material, the U-Pb results reproduce recommended values within uncertainty or yield almost identical dates as those obtained on other accessory minerals from the same location. The Sm-Nd isotopic compositions of the natural titanite crystals are all consistent with values determined by solution methods, demonstrating the reliability and robustness of the *in situ* Sm-Nd laser ablation protocols described herein. We conclude that BLR-1, OLT1, Ontario, MKED1 and T3 titanites have relatively homogeneous Sm-Nd isotope systematics and a reproducible U-Pb isotopic composition and thus can serve as ideal primary reference materials for calibration during *in situ* Sm-Nd analysis and U-Pb dating. Other titanite crystals (YQ-82, T4 and Pakistan) can serve as secondary reference materials for U-Pb and Sm-Nd isotopic microanalysis.

Acknowledgements

This work was financially supported by The National Key R&D Program of China (2016YFE0203000, 2016YFC0600304), the Natural Science Foundation of China (Grants 41525012, 41773047, 41673061, 41473012, 91755207, 41602059, 41802058 and 41273044) and 111 Project (B18048). We are grateful to L.M. Heaman, J.N. Aleinikoff, A.K. Kennedy and C. Spandler for providing the Khan, BLR-1, OLT1 and MKED1 reference titanites, respectively. Zhang H.F. (YQ-82), Deng X.D. (NW-IOA and Pakistan) and Li J.W. (TLS-36) are thanked for providing the titanite samples. We thank Xie L.W., Huang C., Sun J.F., Mao Q., Zhang D., Yang M. and Zhao H. for their assistance with *in situ* analysis and data reduction. The comments of two anonymous reviewers helped to clarify our arguments and are gratefully acknowledged.

References

Aleinikoff J.N., Wintsch R.P., Tollo R.P., Unruh D.M., Fanning C.M. and Schmitz M.D. (2007)
Ages and origins of rocks of the Killingworth dome, south-central Connecticut: Implications for the tectonic evolution of southern New England. **American Journal of Science, 307**, 63–118.

Amelin Y. (2009)
Sm-Nd and U-Pb systematics of single titanite grains. **Chemical Geology, 261**, 53–61.

Banerjee N.R., Simonetti A., Furnes H., Muehlenbachs K., Staudigel H., Heaman L. and Van Kranendonk M.J. (2007)
Direct dating of Archean microbial ichnofossils. **Geology, 35**, 487–490.

Bonamici C.E., Fanning C.M., Kozdon R., Fournelle J.H. and Valley J.W. (2015)
Combined oxygen-isotope and U-Pb zoning studies of titanite: New criteria for age preservation. **Chemical Geology, 398**, 70–84.

Boynton W.V. (1984)
Geochemistry of the rare earth elements: Meteorite studies. **In: Henderson P. (ed.), Rare earth element geochemistry. Elsevier (Amsterdam)**, 63–114.

Burn M., Lanari P., Pettke T. and Engi M. (2017)
Non-matrix-matched standardisation in LA-ICP-MS analysis: General approach, and application to allanite Th-U-Pb dating. **Journal of Analytical Atomic Spectrometry, 32**, 1359–1377.

Cao M.J., Qin K.Z., Li G.M., Evans N.J. and Jin L.Y. (2015)
In situ LA-(MC)-ICP-MS trace element and Nd isotopic compositions and genesis of polygenetic titanite from the Baogutu reduced porphyry Cu deposit, Western Junggar, NW China. **Ore Geology Reviews, 65**, 940–954.

Cherniak D.J. (1993)
Lead diffusion in titanite and preliminary results on the effects of radiation damage on Pb transport. **Chemical Geology, 110**, 177–194.

Cherniak D.J. (1995)
Sr and Nd diffusion in titanite. **Chemical Geology, 125**, 219–232.

Chew D.M., Petrus J.A. and Kamber B.S. (2014)
U-Pb LA-ICP-MS dating using accessory mineral standards with variable common Pb. **Chemical Geology, 363**, 185–199.

Chu Z.Y., Chen F.K., Yang Y.H. and Guo J.H. (2009)
Precise determination of Sm, Nd concentrations and Nd isotopic compositions at the nanogram level in geological samples by thermal ionization mass spectrometry. **Journal of Analytical Atomic Spectrometry, 24**, 1534–1544.

Corfu F. (1996)
Multistage zircon and titanite growth and inheritance in an Archean gneiss complex, Winnipeg River Subprovince, Ontario. **Earth and Planetary Science Letters, 141**, 175–186.

references

Cosca M.A., Mezger K. and Essene E.J. (1998)
The Baltica-Laurentia connection: Sveconorwegian (Grenvillian) metamorphism, cooling, and unroofing in the Bamble Sector, Norway. **The Journal of Geology**, **106**, 539–552.

Dahlgren S., Bogoch R., Magaritz M. and Michard A. (1992)
Hydrothermal dolomite marbles associated with charnockitic magmatism in the Proterozoic Bamble Shear Belt, south Norway. **Contribution to Mineralogy and Petrology**, **113**, 394–409.

Dubois J.C., Retali G. and Cesario J. (1992)
Isotopic analysis of rare earth elements by total vaporization of samples in thermal ionization mass spectrometry. **International Journal of Mass Spectrometry and Ion Processes**, **120**, 163–177.

Engvik A.K., Bingen B. and Solli A. (2016)
Localized occurrences of granulite: *P-T* modeling, U-Pb geochronology and distribution of early-Sveconorwegian high-grade metamorphism in Bamble, South Norway. **Lithos**, **240–243**, 84–103.

Fisher C.M., McFarlane C.R.M., Hanchar J.M., Schmitz M.D., Sylvester P.J., Lam R. and Longerich H.P. (2011)
Sm-Nd isotope systematics by laser ablation-multicollector-inductively coupled plasma-mass spectrometry: Methods and potential natural and synthetic reference materials. **Chemical Geology**, **284**, 1–20.

Foster G.L. and Vance D. (2006)
In situ Nd isotopic analysis of geological materials by laser ablation MC-ICP-MS. **Journal of Analytical Atomic Spectrometry**, **21**, 288–296.

Frost B.R., Chamberlain K.R. and Schumacher J.C. (2000)
Sphene (titanite): Phase relations and role as a geochronometer. **Chemical Geology**, **172**, 131–148.

Fu Y., Sun X., Zhou H., Lin H. and Yang T. (2016)
In-situ LA-ICP-MS U-Pb geochronology and trace elements analysis of polygenetic titanite from the giant Beiya gold-polymetallic deposit in Yunnan Province, Southwest China. **Ore Geology Reviews**, **77**, 43–56.

Gregory C.J., McFarlane C.R.M., Hermann J. and Rubatto D. (2009)
Tracing the evolution of calc-alkaline magmas: *In-situ* Sm-Nd isotope studies of accessory minerals in the Bergell Igneous Complex, Italy. **Chemical Geology**, **260**, 73–86.

Griffin W.L., Powell W.J., Pearson N.J. and O'Reilly S.Y. (2008)
GLITTER: Data reduction software for laser ablation ICP-MS. In: **Sylvester P. (ed.), Laser ablation-ICP-MS in the Earth sciences: Current practices and outstanding issues. Mineralogical Association of Canada Short Course**, **40**, 308–311.

Heaman L.M. (2009)
The application of U-Pb geochronology to mafic, ultramafic and alkaline rocks: An evaluation of three mineral standards. **Chemical Geology**, **261**, 43–52.

Horstwood M.S.A., Košler J., Gehrels G., Jackson S.E., McLean N.M., Paton C., Pearson N.J., Sircombe K., Sylvester P., Vermeesch P., Bowring J.F., Condon D.J. and Schoene B. (2016)
Community-derived standards for LA-ICP-MS U-(Th-)Pb geochronology – Uncertainty propagation, age interpretation and data reporting. **Geostandards and Geoanalytical Research**, **40**, 311–332.

Huang C., Yang Y.H., Yang J.H. and Xie L.W. (2015)
In situ simultaneous measurement of Rb-Sr/Sm-Nd or Sm-Nd/Lu-Hf isotopes in natural minerals using laser ablation multi-collector ICP-MS. **Journal of Analytical Atomic Spectrometry**, **30**, 994–1000.

Huyskens M.H., Yin Q.Z., Li Q.L., Li X.H., Liu Y. and Tang G.Q. (2016)
In search of new monazite and titanite standard minerals for *in situ* U-Pb geochronology. **47th Lunar and Planetary Science Conference**, 2369.

Iizuka T., Eggins S.M., McCulloch M.T., Kinsley L.P.J. and Mortimer G.E. (2011)
Precise and accurate determination of $^{147}Sm/^{144}Nd$ and $^{143}Nd/^{144}Nd$ in monazite using laser ablation-MC-ICP-MS. **Chemical Geology**, **282**, 45–57.

Isnard H., Brennetot R., Caussignac C., Caussignac N. and Chartier F. (2005)
Investigations for determination of Gd and Sm isotopic compositions in spent nuclear fuels samples by MC-ICP-MS. **International Journal of Mass Spectrometry**, **246**, 66–73.

Jacobsen S.B. and Wasserburg G.J. (1980)
Sm-Nd isotopic evolution of chondrites. **Earth and Planetary Science Letters**, **50**, 139–155.

Jiang P., Yang K.F., Fan H.R., Liu X., Cai Y.C. and Yang Y.H. (2016)
Titanite-scale insights into multi-stage magma mixing in Early Cretaceous of NW Jiaodong terrane, North China Craton. **Lithos**, **258–259**, 197–214.

Kennedy A.K., Kamo S.L., Nasdala L. and Timms N.E. (2010)
Grenville skarn titanite: Potential reference material for SIMS U-Th-Pb analysis. **The Canadian Mineralogist**, **48**, 1423–1443.

Kinny P.D., McNaughton N.J., Fanning C.M. and Mass R. (1994)
518 Ma sphene (titanite) from the Khan Pegmatite, Namibia, southwest Africa: A potential ion microprobe standard. **Abstract presented at the 8th International Conference on Geochronology, Cosmochronology and Isotope Geology. U.S. Geological Survey, Circular 1107**, 171.

Kirkland C.L., Spaggiari C.V., Johnson T.E., Smithies R.H., Danišík M., Evans N., Wingate M.T.D., Clark C., Spencer C., Mikucki E. and McDonald B.J. (2016)
Grain size matters: Implications for element and isotopic mobility in titanite. **Precambrian Research**, **278**, 283–302.

references

Kirkland C.L., Fougerouse D., Reddy S.M., Hollis J. and Saxey D.W. (2018)
Assessing the mechanisms of common Pb incorporation into titanite. Chemical Geology, 483, 558–566.

Kohn M.J. (2017)
Titanite petrochronology. Reviews in Mineralogy and Geochemistry, 83, 419–441.

Kowallis B.J., Christiansen E.H. and Griffen D.T. (1997)
Compositional variations in titanite. Geological Society of America Program with Abstracts, 29, 402.

Li J.W., Deng X.D., Zhou M.F., Liu Y.S., Zhao X.F. and Guo J.L. (2010)
Laser ablation ICP-MS titanite U-Th-Pb dating of hydrothermal ore deposits: A case study of the Tonglushan Cu-Fe-Au skarn deposit, SE Hubei Province, China. Chemical Geology, 270, 56–67.

Li Y., Yang Y.H., Jiao S.J., Wu F.Y., Yang J.H., Xie L.W. and Huang C. (2015)
In situ determination of hafnium isotopes from rutile using LA-MC-ICP-MS. Science China Earth Sciences, 58, 2134–2144.

Lin J., Liu Y.S., Yang Y.H. and Hu Z.C. (2016)
Calibration and correction of LA-ICP-MS and LA-MC-ICP-MS analyses for element contents and isotopic ratios. Solid Earth Sciences, 1, 5–27.

Liu Z.C., Wu F.Y., Yang Y.H., Yang J.H. and Wilde S.A. (2012)
Neodymium isotopic compositions of the standard monazites used in U-Th-Pb geochronology. Chemical Geology, 334, 221–239.

Liu Y.N., Fan Y., Zhou T.F., Zhang L.J., White N.C. and Hong H.L. (2018)
LA-ICP-MS titanite U-Pb dating and mineral chemistry of the Luohe magnetite-apatite (MA)-type deposit in the Lu-Zong volcanic basin, Eastern China. Ore Geology Reviews, 92, 284–296.

Ludwig K.R. (2003)
ISOPLOT 3.0 – A geochronological toolkit for Microsoft Excel. Berkeley Geochronology Center Special Publication, No. 4, 70pp.

Lugmair G.W. and Marti K. (1978)
Lunar initial $^{143}Nd/^{144}Nd$: Differential evolution of the lunar crust and mantle. Earth and Planetary Science Letters, 39, 349–357.

Marsh J.H. and Smye A.J. (2017)
U-Pb systematics and trace element characteristics in titanite from a high-pressure mafic granulite. Chemical Geology, 466, 403–416.

Mazdab F.K. (2009)
Characterization of flux-grown trace-element-doped titanite using the high-mass-resolution ion microprobe (SHRIMP-RG). The Canadian Mineralogist, 47, 813–831.

McFarlane C.R.M. and McCulloch M.T. (2007)
Coupling of *in-situ* Sm-Nd systematics and U-Pb dating of monazite and allanite with applications to crustal evolution studies. Chemical Geology, 245, 45–60.

Nijland T.G., Harlov D.E. and Andersen T. (2014)
The Bamble Sector, South Norway: A review. Geoscience Frontiers, 5, 635–658.

Olierook H.K.H., Taylor R.J.M., Erickson T.M., Clark C., Reddy S.M., Kirland C.L., Jahn I. and Barham M. (2018)
Unravelling complex geologic histories using U-Pb and trace element systematics of titanite. Chemical Geology, 54, 105–122.

O'Nions R.K., Hamilton P.J. and Evensen N.M. (1977)
Variations in $^{143}Nd/^{144}Nd$ and $^{87}Sr/^{86}Sr$ ratios in oceanic basalts. Earth and Planetary Science Letters, 34, 13–22.

Prowatke S. and Klemme S. (2005)
Effect of melt composition on the partitioning of trace elements between titanite and silicate melt. Geochimica et Cosmochimica Acta, 69, 695–709.

Rasmussen B., Fletcher I.R. and Muhling J.R. (2013)
Dating deposition and low-grade metamorphism by *in situ* U-Pb geochronology of titanite in the Palaeoproterozoic Timeball Hill Formation, southern Africa. Chemical Geology, 351, 29–39.

Schaltegger U., Brack P., Ovtcharova M., Peytcheva I., Schoene B., Stracke A., Marocchi M. and Bargossi G.M. (2009)
Zircon and titanite recording 1.5 million years of magma accretion, crystallization and initial cooling in a composite pluton (southern Adamello batholith, northern Italy). Earth and Planetary Science Letters, 286, 208–218.

Scott D.J. and St-Onge M.R. (1995)
Constraints on Pb closure temperature in titanite based on rocks from the Ungava orogen, Canada: Implications for U-Pb geochronology and P-T-t path determinations. Geology, 23, 1123–1126.

Simonetti A., Heaman L.M., Chacko T. and Banerjee N.R. (2006)
In situ petrographic thin section U-Pb dating of zircon, monazite, and titanite using laser ablation-MC-ICP-MS. International Journal of Mass Spectrometry, 253, 87–97.

Spandler C., Hammerli J., Sha P., Hilbert-Wolf H., Hu Y., Roberts E. and Schmitz M. (2016)
MKED1: A new titanite standard for *in situ* analysis of Sm-Nd isotopes and U-Pb geochronology. Chemical Geology, 425, 110–126.

Spencer K.J., Hacker B.R., Kylander-Clark A.R.C., Andersen T.B., Cottle J.M., Stearns M.A., Poletti J.E. and Seward G.G.E. (2013)
Campaign-style titanite U-Pb dating by laser-ablation ICP: Implications for crustal flow, phase transformations and titanite closure. Chemical Geology, 341, 84–101.

Stacey J.S. and Kramers J.D. (1975)
Approximation of terrestrial lead isotope evolution by a two-stage model. Earth and Planetary Science Letters, 26, 207–221.

references

Storey C.D., Jeffries T.E. and Smith M. (2006)
Common lead-corrected laser ablation ICP-MS U-Pb systematics and geochronology of titanite. Chemical Geology, 227, 37–52.

Sun J.F., Yang J.H., Wu F.Y., Xie L.W., Yang Y.H., Liu Z.C. and Li X.H. (2012)
In situ U-Pb dating of titanite by LA-ICP-MS. Chinese Science Bulletin, 57, 2506–2516.

Tiepolo M., Oberti R. and Vannucci R. (2002)
Trace-element incorporation in titanite: Constraints from experimentally determined solid/liquid partition coefficients. Chemical Geology, 191, 105–119.

Tilton G.R. and Grunenfelder M.H. (1968)
Sphene: Uranium-lead ages. Science, 159, 1458–1461.

Tucker R.D., Råheim A., Krogh T.E. and Corfu F. (1987)
Uranium-lead zircon and titanite ages from the northern portion of the Western Gneiss Region, south-central Norway. Earth and Planetary Science Letters, 81, 203–211.

Wasserburg G.J., Jacousen S.B., DePaolo D.J., Mcculloch M.T. and Wen T. (1981)
Precise determination of Sm/Nd ratios, Sm and Nd isotopic abundances in standard solutions. Geochimica et Cosmochimica Acta, 45, 2311–2323.

Weis D., Kieffer B., Maerschalk C., Barling J., de Jong J., Williams G.A., Hanano D., Pretorius W., Mattielli N., Scoates J.S., Goolaerts A., Friedman R.M. and Mahoney J.B. (2006)
High-precision isotopic characterization of USGS reference materials by TIMS and MC-ICP-MS. Geochemistry, Geophysics, Geosystems, 7, Q08006.

Willigers B.J.A., Baker J.A., Krogstad E.J. and Peate D.W. (2002)
Precise and accurate *in situ* Pb-Pb dating of apatite, monazite, and sphene by laser ablation multiple-collector ICP-MS. Geochimica et Cosmochimica Acta, 66, 1051–1066.

Wu F.Y., Yang Y.H., Xie L.W., Yang J.H. and Xu P. (2006)
Hf isotopic compositions of the standard zircons and baddeleyites used in U-Pb geochronology. Chemical Geology, 234, 105–126.

Xie L., Wang R.C., Chen J. and Zhu J.C. (2010)
Mineralogical evidence for magmatic and hydrothermal processes in the Qitianling oxidized tin-bearing granite (Hunan, South China): EMP and (MC)-LA-ICPMS investigations of three types of titanite. Chemical Geology, 276, 53–68.

Xie L.W., Evans N., Yang Y.H., Huang C. and Yang J.H. (2018)
U-Th-Pb geochronology and simultaneous analysis of multiple isotope systems in geological samples by LA-MC-ICP-MS. Journal of Analytical Atomic Spectrometry, 33, 1600–1615.

Xu L.L., Bi X.W., Hu R.Z., Tang Y.Y., Wang X.S. and Xu Y. (2015a)
LA-ICP-MS mineral chemistry of titanite and the geological implications for exploration of porphyry Cu deposits in the Jinshajiang-Red River alkaline igneous belt, SW China. Mineralogy and Petrology, 109, 181–200.

Xu L., Hu Z.C., Zhang W., Yang L., Liu Y.S., Gao S., Luo T. and Hu S.H. (2015b)
In situ Nd isotope analyses in geological materials with signal enhancement and non-linear mass dependent fractionation reduction using laser ablation MC-ICP-MS. Journal of Analytical Atomic Spectrometry, 30, 232–244.

Xu L., Yang J.H., Yang Y.H., Hu Z.C., Liu Y.S., Wu Y.B., Luo T. and Hu S.H. (2018)
Determination of Sm-Nd isotopic compositions in fifteen geological materials using laser ablation MC-ICP-MS and application to monazite geochronology of metasedimentary rock in the North China Craton. Geostandards and Geoanalytical Research, 42, 379–394.

Yang Y.H., Sun J.F., Xie L.W., Fan H.R. and Wu F.Y. (2008)
In situ Nd isotopic measurement of natural geological materials by LA-MC-ICP-MS. Chinese Science Bulletin, 53, 1062–1070.

Yang Y.H., Wu F.Y., Wilde S.A., Liu X.M., Zhang Y.B., Xie L.W. and Yang J.H. (2009)
In situ perovskite Sr-Nd isotopic constraints on the petrogenesis of the Ordovician Mengyin kimberlites in the North China Craton. Chemical Geology, 264, 24–42.

Yang Y.H., Wu F.Y., Xie L.W. and Zhang Y.B. (2010)
High-precision measurements of the $^{143}Nd/^{144}Nd$ isotope ratio in certified reference materials without Nd and Sm separation by multiple collector inductively coupled plasma-mass spectrometry. Analytical Letters, 43, 142–150.

Yang Y.H., Chu Z.Y., Wu F.Y., Xie L.W. and Yang J.H. (2011)
Precise and accurate determination of Sm, Nd concentrations and Nd isotopic compositions in geological samples by MC-ICP-MS. Journal of Analytical Atomic Spectrometry, 26, 1237–1244.

Yang Y.H., Wu F.Y., Chu Z.Y., Xie L.W. and Yang J.H. (2013)
High-precision simultaneous determination of $^{147}Sm/^{144}Nd$ and $^{143}Nd/^{144}Nd$ ratios in Sm-Nd mixtures using multicollector inductively coupled plasma-mass spectrometry and its comparison to isotope dilution analysis. Spectrochimica Acta Part B, 79–80, 82–87.

Yang Y.H., Wu F.Y., Yang J.H., Chew D.M., Xie L.W., Chu Z.Y., Zhang Y.B. and Huang C. (2014)
Sr and Nd isotopic compositions of apatite reference materials used in U-Th-Pb geochronology. Chemical Geology, 385, 35–55.

Supporting information

The following supporting information may be found in the online version of this article:

Figure S1. Mineral inclusions in YQ-82 titanite crystals with BSE images.

Table S1. Electron probe microanalysis measurement results for titanite materials.

Table S2. Trace element data by LA-ICP-MS.

Table S3. Titanite U-Pb isotopic data from LA-ICP-MS in this study.

Table S4. Samarium and Nd measurement results for titanite materials.

Table S5. Common Pb (f_{206}), U and total REE contents in different titanites.

This material is available from: http://onlinelibrary.wiley.com/doi/10.1111/ggr.12264/abstract (This link will take you to the article abstract).